Six-year observations of aerosol optical properties at a southern African grassland savannah site

Venter, Marcell

2020-06-01

Venter , M , Beukes , J P , van Zyl , P G , Vakkari , V , Virkkula , A , Josipovic , M , Kulmala , M & Laakso , L 2020 , ' Six-year observations of aerosol optical properties at a southern African grassland savannah site ' , Atmospheric Environment , vol. 230 , 117477 . https://doi.org/10.1016/j.atmosenv

http://hdl.handle.net/10138/342978
https://doi.org/10.1016/j.atmosenv.2020.117477

Six-year observations of aerosol optical properties at a southern African grassland savannah site

Marcell Venter[1], Johan Paul Beukes*[1], Pieter Gideon van Zyl[1], Ville Vakkari[1,2], Aki Virkkula[2], Miroslav Josipovic[1], Markku Kulmala[3], Lauri Laakso[1,2]

[1]Atmospheric Chemistry Research Group, Chemical Resource Beneficiation, North-West University, Potchefstroom, South Africa
[2]Finnish Meteorological Institute, Helsinki, Finland
[3]Department of Physics, PO Box 64, FIN-00014, University of Helsinki, Finland

Correspondence to: JP Beukes; e-mail: paul.beukes@nwu.ac.za; Postal address: Private Bag X6001, South Africa, Potchefstroom, 2520; Tel: +27 18 299 2337; Fax: +27 18 299 2350 (fax)

Highlights

- A six-year, ground level aerosol optical property dataset is presented.
- Well-defined seasonal and diurnal patterns were evident for the optical properties.
- Auto-generated source maps were used to explain results within a regional context.
- Air masses passing over the Karoo region represented the most natural background.
- Anthropogenic influences were evident in air masses passing over all other regions.

Abstract

Atmospheric aerosols have a significant effect on earth's radiative budget, particularly on regional scales. This paper presents a ~6 year, *in situ*, ground level aerosol scattering and absorption dataset, measured at a background site strategically positioned to enable differentiation of the effect of anthropogenic, population density and open biomass burning activities on a regional scale. Relatively well-defined seasonal and diurnal patterns were observed for all the aerosol optical properties, i.e. scattering coefficient (σ_{SP}), absorption coefficient (σ_{AP}), single scattering albedo (ω_0) and Ångström exponent of scattering (α_{SP}). These patterns were explained by considering southern African specific sources and metrological conditions. Using a receptor modelling method (auto-generated source maps) it was found that air masses that had higher σ_{SP}, σ_{AP} and ω_0, and lower α_{SP}, if compared with the relatively clean background, passed over source regions with significant industrial or other anthropogenic activities, higher population density, re-circulation of polluted air masses and higher open biomass burning frequency. To quantify differences, four source regions were defined, i.e. Karoo, Kalahari, anti-cyclonic recirculation pattern and the industrial hub of South Africa. Air masses that had passed over the Karoo source region represented the cleanest regional background conditions, while air masses that had passed either over the industrial hub and/or the anti-cyclonic recirculation pattern represented the most significant anthropogenically impacted, as indicated by the aerosol optical properties. The ω_0 medians of air masses that had passed over the Karoo (0.80–0.86) were 9, 12 and 7 % lower than in air masses that had passed over source regions with the highest ω_0 median, in the warmest/wettest, coldest, and driest, peak open biomass burning periods, respectively.

Keywords: Aerosol scattering coefficient (σ_{SP}), Absorption coefficient (σ_{AP}), Single scattering albedo (ω_0), Ångström exponent of scattering (α_{SP}), Welgegund measurement station

1 Introduction

Atmospheric aerosols can have a significant effect on the earth's radiative budget in two ways: particles that directly scatter and absorb shortwave and long wave radiation, and particles that indirectly influence physical properties and lifetimes of clouds by serving as cloud condensation nuclei (e.g. Boucher et al., 2013). However, the atmospheric lifetime of aerosols is in general much shorter than the long-lived greenhouse gases; therefore, the climatic impacts of aerosols are particularly important on regional scales (e.g. Forster et al., 2007). Consequently, long-term, regional scale and high temporal resolved measurements are required in order to determine aerosol climatic impacts and to improve the uncertainties associated with these impacts.

Although Africa is an important source region for numerous gas and aerosol species, it is one of the least studied continents, possibly since most African countries can be regarded as developing (lacking resources). Southern Africa is an important sub source region, with open biomass burning being a major concern due its general air quality, health, visibility and climate impacts. Open biomass burning in this region includes grassland, savannah and forest fires, as well as agricultural burning, which combined produce significant amounts of aerosols especially in the dry season (Vakkari et al., 2018, 2014; Mafusire et al., 2016;). Domestic combustion (i.e. cooking and household space heating) also contributes significantly to the atmospheric aerosol load, especially near informal settlements (low-income households that erect housing from any available material) (Chiloane et al., 2017; Hersey et al., 2015). Within southern Africa, South Africa has the largest economy, with numerous sources that emit aerosols as primary pollutants. Major anthropogenic point sources in South Africa include an array of very large coal-fired power stations and petrochemical operations that do not de-SO_x or de-NO_x their off gas (Pretorius et al., 2015), and large mining and pyro-metallurgical industries (e.g. Loock-Hattingh et al., 2015; Hirsikko et al., 2012). Secondary formed aerosols is also very prevalent, with regional new particle formation frequencies measured in the South African interior being the highest ever recorded internationally (Nieminen et al., 2018).

Notwithstanding the significance of the climatic effect of aerosols and the importance of South Africa (and southern Africa in general) within a regional and global atmospheric science perspective, few papers have been published in the peer reviewed public domain on aerosol optical properties for this region. Most of these papers used vertical and/or remote sensing techniques to obtain aerosol optical data (Kumar et al., 2014; Queface et al., 2011; Campbell et al., 2003; Eck et al., 2003; McGill et al., 2003; Formenti et al., 2002; Diner et al., 2001), were mostly focussed only on open biomass burning (Campbell et al., 2003; Eck et al., 2003; McGill et al., 2003; Diner et al., 2001) and were generally based on short measurement periods during the SAFARI 2000 campaign (Swap et al., 2003). As far as the authors could assess, the Laakso et al. (2012) paper is the only study to date for South Africa where ground level, multi-year aerosol optical properties, based on *in situ* aerosol absorption and scattering measurements, have been published. Although this paper made a significant contribution, it was a general paper that considered various aerosol and gas measurements and therefore did not focus specifically on explaining aerosol optical properties in detail. Also, in this paper no diurnal patterns were presented and possible source explanations were quite general. Additionally, the measurements site (i.e. Elandsfontein) was situated in the internationally well-known NO_2 hotspot visible with satellite observations (Lourens et al., 2012), implying that the optical data is only representative of this relatively small area (Laakso et al., 2012). In South Africa, the Cape Point Global Atmosphere Watch (GAW) station (e.g. Slemr et al., 2015; Venter et al., 2015; Slemr et al., 2013)

also measures ground level *in situ* aerosol absorption and scattering on a continuous basis, however, as far as the authors could assess results from there have not yet been published in the peer reviewed public domain.

Considering the above-mentioned, studies focussing specifically on ground level aerosol optical properties for South Africa have been lacking. However, resources to operate multiple sites to obtain such data were not available, and is unlikely to become available in the near future. Therefore, continuous aerosol optical measurement were established at Welgegund, a site that enabled assessment of aerosol optical properties on a regional, rather than limited local basis, for South Africa. The general aims of this paper were to introduce the measurements and present initial assessment of the first six years of gathered data. The specific objectives were to contextualise the observed mean/median aerosol optical properties (scattering and absorption coefficients, σ_{SP} and σ_{AP}, single scattering albedo, ω_0, and Ångström exponent of scattering, α_{SP}) within a global context, present and comprehend seasonal and diurnal patterns, as well as contemplate factors influencing aerosol optical properties and possible sources on a regional scale for South Africa.

2 Site description

Measurements were conducted at the Welgegund measurement station (26°34'11.23" S, 26°56'21.44" E, 1480 m.a.s.l.). Welgegund has been introduced in previous papers (Jaars et al., 2016, 2014; Laban et al., 2018; Vakkari et al., 2018, 2015 and 2014; Venter et al., 2018, 2017, 2015; Chiloane et al., 2017; Räsänen et al., 2017; Booyens et al., 2019, 2015), therefore only a synopsis of the site description is given. The location of the Welgegund measurement station is indicated in Fig. 1 along with the main vegetation type biomes and population density of southern Africa. It is situated approximately 100 km southwest of Johannesburg on a commercial farm, and is surrounded by grazed grassland and semi-savannah (Fig. 1), as well as cultivated farmlands. Jaars et al. (2018) presented a detailed vegetation survey within a 60 km radius around Welgegund. There are no significant nearby anthropogenic pollution sources and most of the large point sources are situated to the east, in the sector between north to south-east form Welgegund. The population density is also higher to the east of Welgegund with significantly lower density to the west. Therefore, the sector west of Welgegund (from north to south-east) can be considered as representative of the regional background of the interior of South Africa. However, aged air masses that had passed over the industrialised source regions also occasionally impact Welgegund (Tiitta et al., 2014; Beukes et al., 2013). These source regions include (i) the Johannesburg-Pretoria (Jhb-Pta) megacity with more than 10 million inhabitants (Lourens et al., 2012, 2016), (ii) the western Bushveld Complex that host 11 pyro-metallurgical smelters in less than a 60 km radius (Hirsikko et al., 2012), (iii) the eastern Bushveld Complex that also host a couple of pyro-metallurgical smelters, (iv) the Mpumalanga Highveld where 11 coal-fired power stations, a very large petrochemical producer and several pyro-metallurgical smelters are located in a small geographical area (Lourens et al., 2011; Collet et al., 2010), and (v) the Vaal Triangle that host several chemical and petrochemical operations, a couple of pyro-metallurgical smelters and a coal-fired power station (Fig. 1). It has been proven in numerous previous publications that regional, rather than local sources, determine the atmospheric composition at Welgegund.

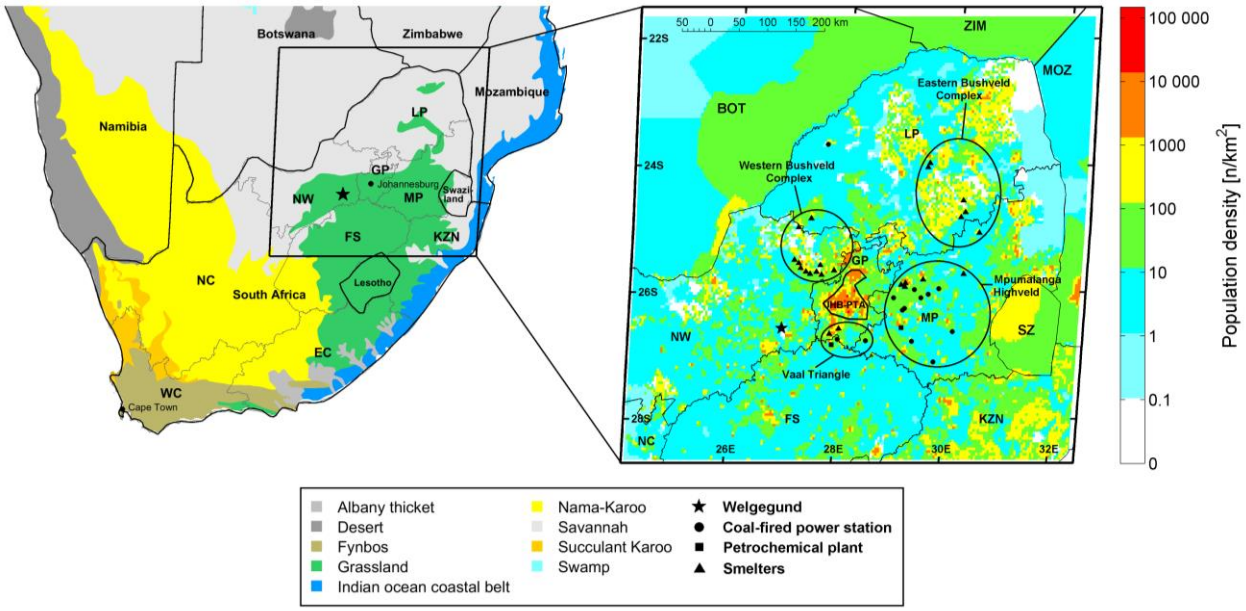

Fig. 1: Southern African map indicating the location of Welgegund in context of vegetation type biomes (Mucina and Rutherford, 2006), major point sources in the interior of South Africa and the Jhb-Pta megacity. The population density is also indicated in the zoomed-in area (CIESIN, 2019). Province abbreviations: WC – Western Cape, NC – Northern Cape, EC – Eastern Cape, FS – Free State, NW – North West, GP – Gauteng Province, LP – Limpopo Province, MP – Mpumalanga Province, KZN – KwaZulu-Natal.

3 Materials and methods

3.1 Measurement equipment, site maintenance and data quality assurance

The Welgegund measurement station is most likely the most comprehensively equipped continuously operating atmospheric monitoring station in the South African interior (Beukes et al., 2015). Light absorption was measured at a sample flow of 6.0 L min^{-1} with a Multi-Angle Absorption Photometer (MAAP) (model 5012 Thermo Fisher Scientific Inc.) at a wavelength of 637 nm. The MAAP measures light absorption but reports equivalent black carbon (eBC) (definitions according to Petzold et al. 2013) concentrations by using the absorption mass efficiency 6.6 m^2 g^{-1}. By multiplying the eBC concentrations by the absorption mass efficiency the light absorption coefficient (σ_{AP}) can be calculated at 637 nm. Absorption uncertainty is estimated to be approximately 12% (Petzold et al., 2005). Light scattering was measured at a sample flow rate of 2.7 L min^{-1} with a three wavelength Nephelometer (Ecotech Aurora 3000) at 450, 525 and 635 nm. The scattering uncertainty is estimated as 10%, after truncation correction (Müller et al., 2011a). Particulate matter concentration with an aerodynamic diameter $\leq$ 10 µm (PM_{10}) was measured with a synchronised hybrid ambient real-time particulate (SHARP) monitor (model 5030, Thermo Fisher Scientific Inc.). All three the afore-mentioned instruments had a common PM_{10} sample inlet. After the inlet, the sampled airflow was split into three with custom-built splitters to maintain isokinetic flow, as far as practically possible. Thereafter, the sampled air of each instrument passed through a customised Nafion™ drier to keep relatively humidity (RH) < 40%, before entering the instrument. The Nafion™ dryers were operated with counter current, partially dry compressed air, from an oil-less compressor system. Data points with RH $\geq$ 40% were removed from the dataset during data cleaning/quality assurance procedures. Ancillary data, such as meteorological parameters (e.g. rain intensity, relative humidity (RH), temperature, as well as wind speed and direction), as well as trace gas concentrations and non-optical aerosol measurements were conducted, as relatively recently summarised by Beukes et al. (2015).

The measurements were undertaken from 1 September 2011 to 30 November 2016. Beukes et al. (2015) described site maintenance and data quality assurance procedures applied for Welgegund, therefore it is not repeated here. However, since these authors did not specify the Nephelometer calibration, it is summarised. The Nephelometer calibration was checked once a week with a HEPA filter (zero) and CO_2 (span). If the instrument response was more than 10 % off, a full calibration was conducted. Between calibrations the readings were corrected for span and zero drift assuming that the drift is linear between calibration checks. All the data (for all instruments) reported in this study was recorded at 1 min intervals. This high resolution 1 min data was converted to 15 min averages, after quality assurance procedures were applied (as specified by Beukes et al., 2015) and only if at least two thirds of the 1 min data were available.

3.2 Aerosol optical calculations

Procedures previously described by Laakso et al. (2012) were used to calculate the various optical parameters. Firstly the σ_{SP} was corrected for temperature (273°K) and pressure (1013 m bar) (i.e. standard temperature and pressure, STP), to correlated with the σ_{AP}, which was also reported at STP. As previously stated (Section 3.1), the MAAP instrument measures light absorption but reports eBC by using the absorption mass efficiency 6.6 m^2 g^{-1}. By multiplying the eBC concentrations by the absorption mass efficiency, σ_{AP} values were calculated at 637 nm. The Nephelometer truncation error was corrected according to Müller et al. (2011b). Thereafter, α_{SP} was calculated for the entire wavelength range (450, 525, 635 nm), by fitting the logarithm of the σ_{SP} and the respective wavelengths to Eq (1):

$$\ln(\sigma_{SP}, \lambda) = -\alpha_{SP} \ln(\lambda) - C \quad (1)$$

where C is a constant that is not relevant to this work. The α_{SP} was then used to logarithmically interpolate the wavelength of σ_{SP} to correlate with that of the σ_{AP}, measured with the MAAP at λ = 637 nm (Müller et al., 2011b). Therefore, σ_{SP} and σ_{AP} reported in this paper will be for λ = 637 nm. The ω_0 can be defined as:

$$\omega_0 = \frac{\sigma_{SP}}{(\sigma_{SP}+\sigma_{AP})} \quad (2)$$

at 637 nm (Gong et al., 2015, Montille et al., 2011). The α_{SP} can be used as a qualitative indicator of particle size distribution (Schuster et al., 2006; Ångström, 1929). Small values (α_{SP} <~ 1) indicate coarse mode particles (radii >~ 0.5 µm) that are associated with for instance sea salt and dust particles and large values (α_{SP} >~ 2) indicate fine mode particles (radii <~ 0.5 µm) that are typically associated with biomass burning and anthropogenic emissions (Schuster et al., 2006; Eck et al., 1999). The interpretation of α_{SP} is not unambiguous, however, as previously indicated (Shen et al., 2018; Virkkula et al., 2011; Garland et al., 2008) it is more applicable to the interpretation of volume or mass mean diameters, than number mean diameters. A limitation of the Nephelometer used in this study, which was an early Ecotech Aurora 3000 model (year 2007) fitted with an improved light source, was that backscattering was not measured. Therefore, the asymmetry parameter (e.g. Yu et al. 2016; Moosmüller and Ogren, 2017) could not be calculated.

3.3 Ancillary data and methods

The Hybrid Single-Particle Lagrangian Integrated Trajectory (HYSPLIT) model (version 4.8) of the National Oceanic and Atmospheric Administration (NOAA) Air Resources Laboratory (ARL) was used to determine air mass histories (Draxler and Hess, 2004), using the 1° resolution GDAS meteorological data archive (GDAS,

2019). All back trajectories were calculated for 96-hours backwards, arriving hourly at Welgegund with an arrival height of 100 m. The accuracy of calculated trajectories significantly depends on the quality of the meteorological data used (Stohl, 1998). Uncertainties associated with a single trajectory calculated in the manner presented here are estimated as 15 to 30% of the trajectory distance travelled (Stohl, 1998; Riddle et al., 2006). For studying regional patterns and using a large dataset this accuracy is sufficient. Further, deductions in this paper were never made based on a single trajectory, but always on multiple (hundreds or thousands) trajectories. When hundreds, or thousands of trajectories are drawn on a map, it is difficult to identify the main air mass movement pattern(s), due to the overlap of trajectories. Therefore, overlay back trajectory maps, as previous introduced (e.g. Venter et al. 2015, 2012), were drawn in such cases. In these maps a colour code was used to indicate the percentage of trajectories passing over 0.2 × 0.2° grid cells superimposed over the region of interest, with dark blue and red indicating the lowest and highest number of trajectory overpasses, respectively. In addition, a technique introduced by Vakkari et al. (2011, 2013) was used to connect air mass history and the optical properties considered in this paper. This was done by defining a 0.5 × 0.5° grid over the southern African map. For each calculated trajectory, grid cells over which the trajectory passed, were assigned the hourly mean of the observed optical property measured at Welgegund. Therefore, for multiple trajectories the value in each grid cell represented the mean of the optical property observed for all the trajectories passing over that grid cell. A minimum of 40 trajectory overpasses per grid cell was required, in order to ensure that the results are statistical reliability. Vakkari et al. (2011, 2013) demonstrated that this method can be used to identify source areas or regions for atmospheric species measured at sites that not in close proximity to large point sources. In this paper, such maps were referred to as auto-generated source maps. This method can be considered as a receptor modelling method. Some receptor modelling methods, such as conditional bivariate probability function (CBPF) using wind parameters (e.g. Uria-Tellaetxe and Carslaw, 2014; Tian et al., 2019), are good to identify nearby/local sources. However, the method applied in this paper (auto-generated source maps) is not effective to account for nearby/local sources, but is excellent at giving a regional perspective, which was one of the main objectives of this paper (see Section 1).

Fire locations were determined with the MODIS collection 5 burned area product (Roy et al., 2008) and results expressed as gridded 500 m pixels as specified in the MODIS user manuals (Boschetti et al. 2009, 2013).

4 Results

4.1 Meteorological data and open biomass burning frequencies

In Fig. S1 the median, as well as 25th and 75th percentiles, of the monthly temperature (Fig. S1a), relative humidity (RH) (Fig. S1b) and cumulative rain (Fig. S1c) are presented for the entire sampling period. From these figures seasonal variations for all the meteorological parameters are evident. Relatively high daily temperatures (21^{o} C median) accompanied by higher RH (above 50 %) and higher precipitation (~86 mm month^{-1}) occurred in the warmer months (November–February). However, the cooler months (May–August) received on average almost no precipitation (below ~15 mm month^{-1}), with lower RH (below 50 %) and lower temperatures (10^{o} C median).

Fig. 2a presents MODIS burned area pixel counts within 100 and 250 km radii around Welgegund for the full calendar years covered by the measurement campaign. As is evident from this data (Fig. 2a), the previously presented lack of rain during the dry season (May–mid-October, Fig. S1c) contribute significantly to open biomass burning, whereas such fires are to a large degree prevented during the wet season (mid-October–April). According

to Archibald et al. (2008), availably of vegetation to serve as fuel during open biomass burning and soil moisture, as influenced by the preceding 2 years of rainfall, is likely the most important drivers for open biomass burning frequency and spatial variation in southern Africa. It is therefore understandable that 2014 that was an above average rainfall year (~101% of regional average; Droughtsa, 2019) had the highest MODIS burn area pixel counts, while 2016 that was a below average rainfall year (~83% of regional average; Droughtsa, 2019) had the lowest (Fig. 2a). The spatial distribution of open biomass burning in southern Africa is illustrated in Fig. 2b, which use 2012 as an example. The lines in this figure divide the southern African map into eastern and western sectors as observed from Welgegund. It is obvious for Fig. 2b that most open biomass burning occurs in the eastern sector, due to the vegetation type biomes (Fig. 1) there being more productive, i.e. produce more vegetation biomass that can burn.

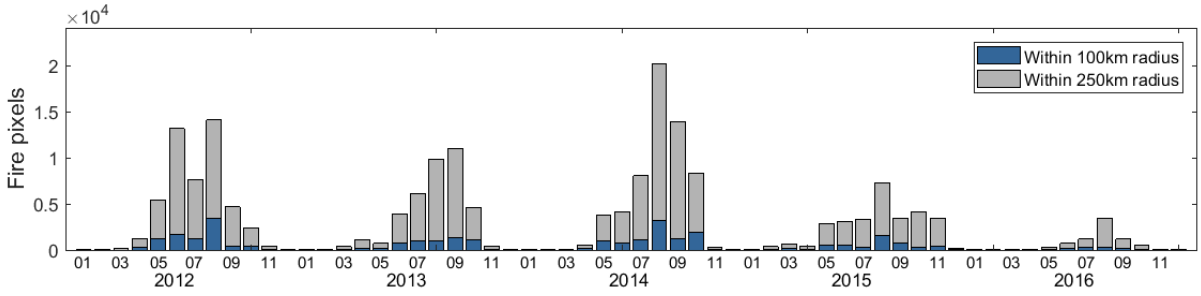

(a)

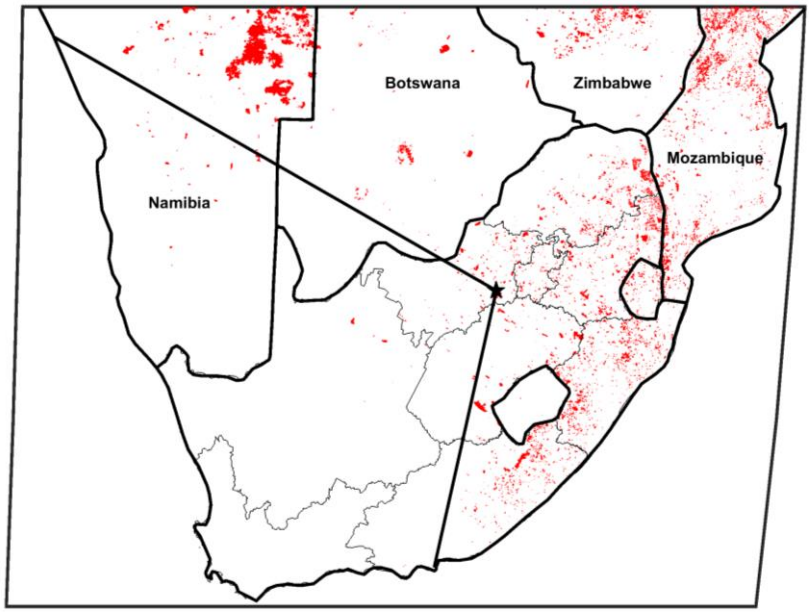

(b)

Fig. 2 (a) MODIS burnt area pixel counts within 100 and 250 km radii around Welgegund, determined with MODIS collection 5 burned area product (Roy et al., 2008), for the entire sampling period and (b) a map of southern Africa indicating MODIS burned area pixel counts observed for 2012. The lines in (b) divide South Africa into eastern and western sectors, with more and less open biomass burning frequencies, respectively, as observed from Welgegund.

4.2 Seasonality of aerosol optical properties

Fig. S2 presents the monthly statistical distribution of the aerosol optical properties for the entire sampling period. This data is condensed in Fig. 3, which presents the monthly statistical distribution of (a) σ_{SP}, (b) σ_{AP}, (c)

ω_0 and (d) α_{SP}, with corresponding months grouped together (i.e. all January data grouped together, Februaries, etc.).

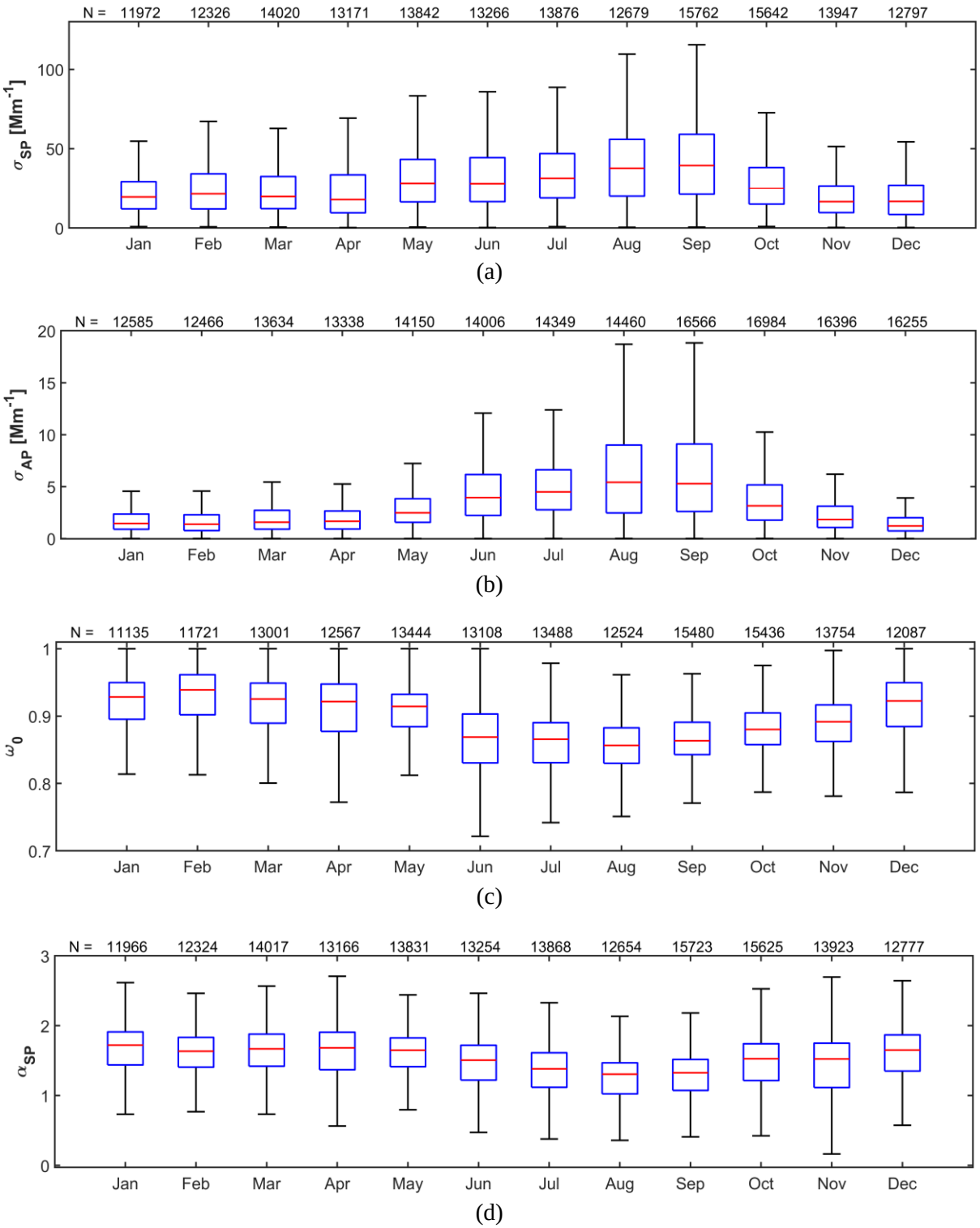

Fig. 3: Monthly statistical distribution of aerosol optical properties measured at Welgegund for the entire sampling period: (a) σ_{SP}, (b) σ_{AP}, (c) ω_0 and (d) α_{SP} with corresponding months grouped together (i.e. all January data grouped together, February, etc.). The red line represents the median, the top and bottom edges of blue boxes the 25 and 75 % percentile and the black whiskers indicates a 99.3 % coverage. The number (N) of 15 min data points represented by each box and whisker is indicated at the top of each graph.

A clear seasonal cycle can be observed for σ_{SP} (Fig. 3a and S2a) and σ_{AP} (Fig. 3b and S2b). The highest medians were observed in the winter and early spring months (June–September), while the lowest medians were recorded during the summer and autumn months (December–April). There are several possible reasons for the relatively well defined σ_{SP} and σ_{AP} seasonal patterns. Domestic space heating occurs mostly during the colder winter months in the South African interior (Chiloane et al., 2017; Hersey et al., 2015; Venter et al., 2012), while domestic cooking is practised irrelevant of the ambient temperatures. The fuel used in domestic combustion depend on the availability and cost of the various fuel types, but low grade coal, wood and paraffin are very typical in the South African context (Pretorius et al., 2015, Census 2011). Also, open biomass burning frequency generally increase during winter and peak in either late winter (August) or early spring (September) (Fig. 2a), which is also the driest period (Fig. S1b and c). Less wet deposition (Fig. S1c), increased anti-cyclonic re-circulation of air masses over the South African interior (Tyson et al., 1996), lower planetary boundary layer (PBL) depths and more prominent thermal inversion layers (Gierens et al., 2019; Korhonen et al., 2014; Garstang et al., 1996; Fig. 4e) during the colder months, all result in aerosol accumulation in the lower atmosphere. Increased wind-blown dust also occurs during the dry season, especially the late dry season (August to mid-October). Additionally, in the cold winter months (Fig. S1a), higher electricity consumption occurs in South Africa (Pretorius et al., 2015), which results in increased SO_2 and NO_x emissions (which are precursors of aerosol sulphate, SO_4^{2-} and nitrate, NO_3^-), from large coal-fired power stations that do not remove such species from their off gas (Pretorius et al., 2015). Considering the afore-mentioned, the observed σ_{SP} and σ_{AP} seasonal patterns are likely a complex combination of increased emissions (e.g. household combustion in winter, open biomass burning during later winter and early spring), trapping of low-level emission during the colder months and reduced wet deposition during late autumn to early spring.

In Fig. 3c and S2c a clear seasonal pattern can be observed for ω_0, with more absorbing aerosols observed during the winter and early spring months, while more scattering aerosols occurred during the summer and early autumn months. This ω_0 seasonality does not correlate with the σ_{SP} and σ_{AP} seasonality, where both these parameters reach maximum values in the winter and/or early spring. The reason why the ω_0 seasonality differs from that of σ_{SP} and σ_{AP} is due to the relative larger amplitude difference of the σ_{AP} peak in the late dry season if compared to the corresponding σ_{SP} peak. This is illustrated by the relatively small ratio difference of 2.1 between the average of the three highest (89.2 M m^{-1}) and average of the three lowest (42.8 M m^{-1}) medians of the σ_{SP} per season (Fig. S2a), if compared to the correlating average ratio of 3.6 for σ_{AP} (derived from average of the three highest medians, i.e. 16.1 M m^{-1}, and the average of the three lowest medians, i.e. 4.5 M m^{-1} per season) (Fig. S2b). The reasons for the larger relative amplitude of σ_{AP} compared to the σ_{SP} peak can be due to increased BC emissions from seasonal combustion sources (e.g. open biomass burning and domestic combustion for space heating), as previously indicated (Chiloane et al., 2017; Tiitta et al., 2014). In addition, SO_2 will be converted more effectively to SO_4^{2-} during the higher RH conditions (Seinfeld and Pandis, 2016) in the wet season (Fig. S1b), which will contribute to the σ_{SP} not reducing as much as σ_{AP} during that time of the year. SO_4^{2-} has been proven to be the dominant inorganic ionic aerosol species (Venter et al., 2018; Aurela et al., 2016; Tiitta et al., 2014) and ionic species in rain water (Conradie et al., 2016) in the South African interior.

A seasonal cycle for the α_{SP}, with the highest median and smallest particle size distribution in summer and early autumn months, and lowest median and largest particle size distribution in the winter and early spring months, can be observed in Fig. 3d and S2d. The timing of the minima in α_{SP} correlate with the peak in wind-

blown dust emissions, that is most significant in later winter and early spring (Tyson and Preston-Whyte, 2000). Open biomass burning also peak during this time of the year (Fig. 2a), but is generally emits smaller particles than wind-blown dust (Schuster et al., 2006; Eck et al., 1999). In contrast the summer and early autumn months are not impacted significantly by the afore-mentioned dry season specific emission sources, but are fractionally more affected by secondary aerosol formation that is very prevalent in the South African interior (Nieminen et al., 2018; Vakkari et al., 2015, 2011; Hirsikko et al., 2013, 2012).

4.3 Diurnal patterns of aerosol optical properties

In Fig. 4 average diurnal patterns for each seasons, for all the aerosol optical properties (σ_{SP}, σ_{AP}, ω_0, and α_{SP}) are presented. As is evident from Fig. 4a the σ_{SP} for all seasons peaked in the morning (between 6:45 and 08:15) and early evening (between 17:45 and 19:00). The σ_{AP} for all seasons (Fig. 4b) indicated similar patterns during the morning, but did not specifically peak in the early evening – it rather increased throughout the night. The afore-mentioned σ_{SP} and σ_{AP} diurnal patterns clearly indicate the influence of the PBL. Gierens et al. (2019) presented the evolution of layers observed in the PBL for the different seasons at Welgegund. In Fig. 4e the average PBL diurnal patterns for summer (DJF) and winter (JJA) are presented – these two seasons represent the extreme cases. In both seasons the average mixed layer depth grew from just after sunrise to a maximum (approximately 2.3 and 1.9 km, in summer and winter, respectively) in late afternoon (Gierens et al., 2019). The increase in the mixed layer depth after sunrise (Fig. 4e) co-inside with decreased σ_{SP} and σ_{AP} (Fig. 4a and b). After sunset, the mixed layer depth decrease (Fig. 4e), which co-inside with increased σ_{SP} and σ_{AP} (Fig. 4a and b), with the exception of the peak observed around 18:00 in σ_{SP} (Fig. 4a). Additionally, after sunset a stable layer (depicted as DJF-S and JJA-S, in Fig. 4e) forms, which is most likely due to thermal inversion at an approximately mean depth of 100 m. This stable layer traps and concentrates near-surface emissions in a smaller volume (Gierens et al., 2019). This effect is stronger during the colder months, if compared to the warmer months (Gierens et al., 2019). In addition to the PBL, sources that vary diurnally (e.g. domestic combustion for space heating) can also contribute to the observed diurnal patterns.

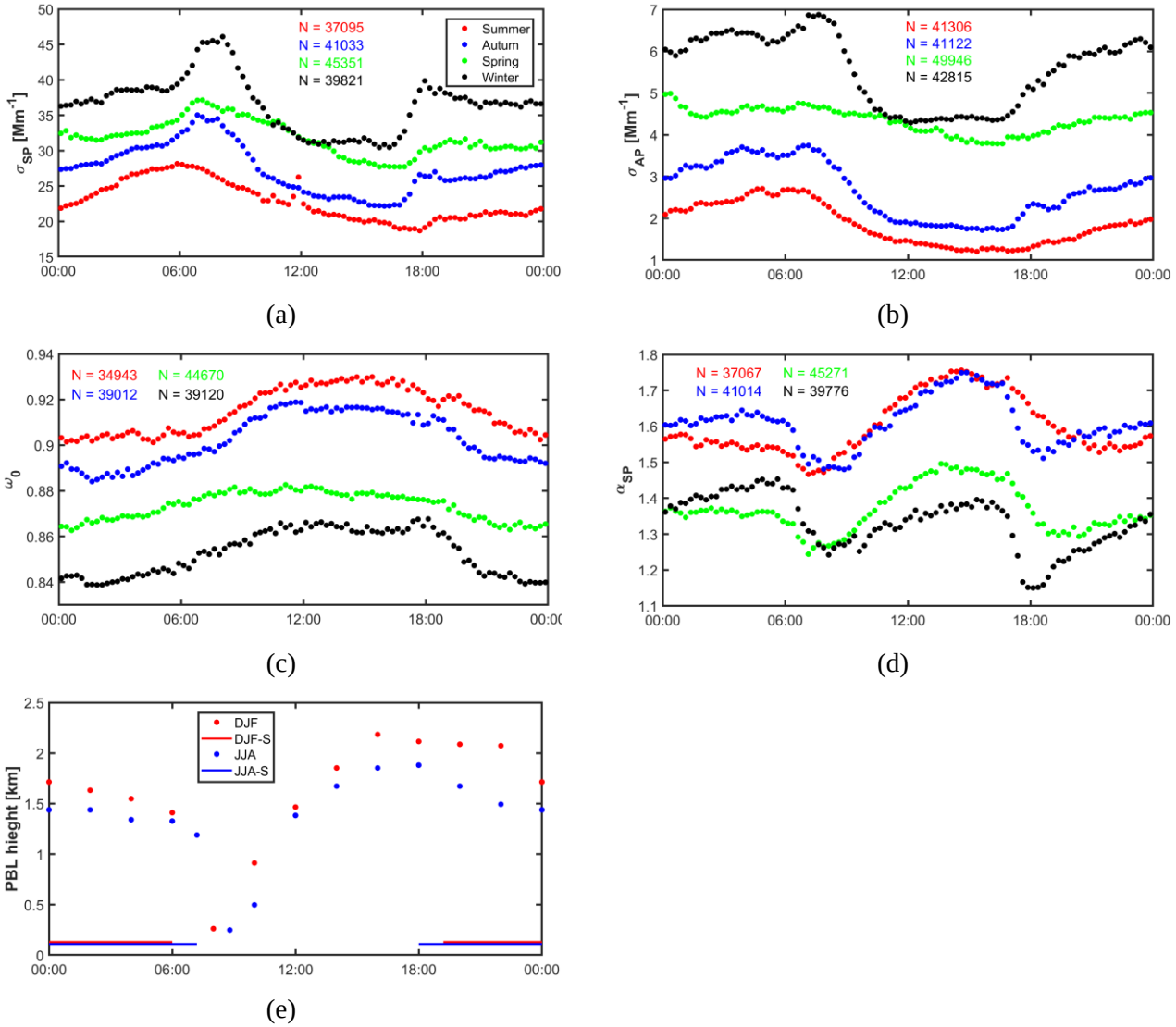

Fig. 4: Average diurnal patterns for the different seasons, for (a) σ_{SP}, (b) σ_{AP}, (c) ω_0 and (d) α_{SP} measured at Welgegund over the entire sampling period (1 September 2011 to 30 November 2016). The number (N) of 15 min data points used to calculate each average diurnal pattern is also indicated with matching colour-coded text. Additionally, in (e) the planetary boundary layer structure for summer (DJF) and winter (JJA), as reported by Gierens et al. (2019) for almost 2 years (1 October 2012 to 31 August 2014) that overlapped with the aerosol sampling reported here, is presented.

Fig. 5 presents the average seasonal diurnal patterns of ω_0, with all seasons indicating similar variations. The ω_0 starts increasing after sunrise in the morning, reaches a maximum at approximately 15:00 and decreases after sunset. Obviously, the ω_0 represent the net effect of σ_{SP} and σ_{AP}, however, there are two reasons that are likely the most significant to explain the more scattering properties of the PM during daytime. Firstly, after sunrise O_3 starts forming due to photochemistry, with associated increased hydroxyl radical ($OH^{\bullet}$) concentrations (Seinfeld and Pandis, 2016) – both resulting in increased oxidising capacity that lead to higher concentrations of scattering species such as organic aerosols (OA) and SO_4^{2-}, which dominate the PM composition in the South African interior (Venter et al., 2018; Aurela et al., 2016; Tiitta et al., 2014). O_3 concentrations at Welgegund usually reach maxima at approximately 1 to 2 hours after maxima solar radiation (Laban et al., 2018), which match the maxima observed in the ω_0 diurnal patterns (Fig. 4c). As far as the author could assess $OH^{\bullet}$ concentrations have not been measured in South Africa, although Gierens et al. (2014) did model diurnal patterns thereof. Secondly, the break-up of low-level inversion layers and growth of the mixed layer in the PBL (Gierens et al., 2019, Fig. 4e) after sunrise, result

in downward mixing of SO_4^{2-} that had formed as a result of long range SO_2 transport. In South Africa SO_2 is mostly emitted form high stacks (with heights of >200m being common, ESKOM 2019a and 2019b). Downward mixed SO_2 can then also be oxidised to SO_4^{2-} during daytime. SO_4^{2-} has been linked to secondary aerosol formation in South Africa (Vakkari et al., 2015). In addition to the effect of SO_4^{2-}, the deeper PBL during daytime (Gierens et al., 2019) also dilutes BC emitted mostly from near surface sources (e.g. open biomass burning and domestic combustion).

Considering Fig. 4c further, it is evident that the ω_0 diurnal pattern for spring indicated a similar trend to the other seasons, but with a much less significant amplitude differences. This could be due to the first half of spring (September and early October) being the driest (Fig. S1b). As previously stated, atmospheric moisture is critical for the oxidation of SO_2 to SO_4^{2-}, with significantly less such conversion taking place at RH below 70 % (Seinfeld and Pandis, 2016). Obviously, differences in seasonal circulation patterns could also influence SO_2 and SO_4^{2-} long-range transport, but this was not considered in detail here.

Fig. 4d presents the average seasonal diurnal patterns of α_{SP}. All the seasonal diurnal patterns were similar, with the amplitude changes in winter being the largest and in summer being the smallest. These α_{SP} seasonal diurnal patterns were compared to the corresponding PM_{10} concentration patterns, as indicated in Fig. 5. Form this comparison it is evident that the α_{SP} diurnal patterns are the inverse of the PM_{10} concentration patterns, which make sense considering that α_{SP} is used to indicate particle size (Schuster et al., 2006; Ångström, 1929). Therefore, the PM_{10} patterns needed to be understood. Considering the earlier descriptions of the different layers in the PBL at Welgegund (Gierens et al., 2019), the peaks in PM_{10} observed during the mornings and early evenings had to originate from near-surface sources and/or pollution transported within the PBL that are concentrated due to formation of the very low level thermal inversion at approximately 100 m depth (Gierens et al., 2019). Such low level sources could for instance be domestic combustion, which becomes a more significant source of PM in the South African interior as seasonal ambient average temperatures decrease (Fig. S1a) – due to space heating becoming more important in addition to cooking (Chiloane et al., 2017). Additionally, open biomass burning plumes in southern Africa typically stay within the PBL (Labonne et al., 2007), therefore, it will also be a significant near surface source for Welgegund. Both the afore-mentioned combustion sources emit on average smaller particles, compared to wind-blown dust. Wind-blown dust concentrations tend to peak after midday in the South African interior, due to wind speeds then in general being the highest during all seasons (e.g. Venter et al., 2012).

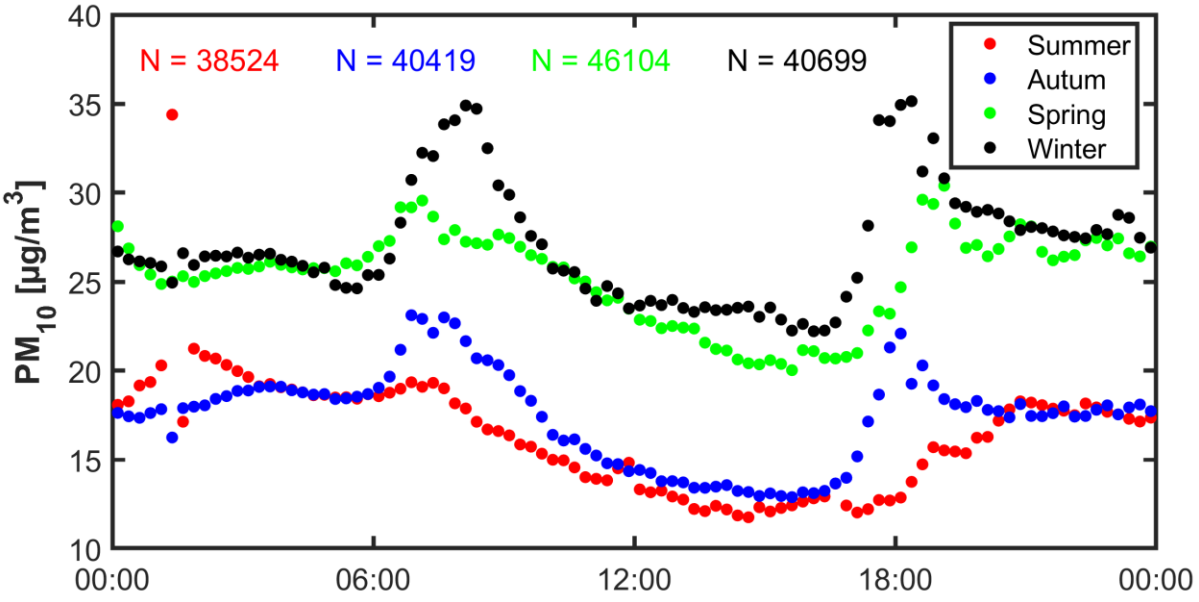

Fig. 5: Average diurnal patterns for the different seasons for PM_{10} measured at Welgegund for the entire sampling period. The number (N) of 15 min data points used to calculate each average diurnal pattern is also indicated with matching colour-coded text.

4.4 Additional source insights

The temporal patterns discussed thus far (Sections 4.2 and 4.3), in association with meteorological and open biomass burning data (Section 4.1), as well as published information has given general insights into possible sources and reasons for the observed aerosol optical properties. However, greater clarity is required; therefore, several more aspects are considered in this section.

An interesting phenomenon that can be observed from Fig. 3d and S2d is that very small values for α_{SP} (approaching zero) are occasionally observed. These observations can be directly correlated with dust storms that are observed at Welgegund. Such small α_{SP} values are typically reported for Sahara and Middle Eastern dust impacted sites (Dubovik et al., 2001). Fig. S3a and S3b present photos of such dust storms approaching a sport field in the city of Potchefstroom (approximately 22.5 km directly from Welgegund) and blowing across a road near Potchefstroom (approximately 30km directly from Welgegund), respectively. One of the most significant source regions of PM_{10} measured at Welgegund is wind-blown dust originating from the eastern Free State, indicated by the circled area in Fig. 6. This figure presents the auto-generated source map (Section 3.3) for PM_{10} concentrations observed at Welgegund. It is understandable that the eastern Free State is a very significant source of dust, since it is the largest maize (staple food in South Africa) producing region in South Africa (DAFF, 2017). Maize production in the Free State province is confined to the eastern part, since the western Free State is situated in the Karoo vegetation type biome (Fig. 1), which is a dry, less productive vegetation type biome where maize is not cultivated commercially. For maize cultivation, the planted fields are typically ploughed in preparation for sowing. This exposes large areas that then become susceptible to wind-blown dust generation. According to Fig. 6 other significant PM_{10} source regions for Welgegund are central Mozambique (which correlates with high fire frequency, Fig. 2b) and the central west coast of Namibia (which is a well-known dust source, Fig. 1) (Bryant, 2003; Barnard, 1998), as well as sea salt aerosols from air masses that travel quickly from the coast.

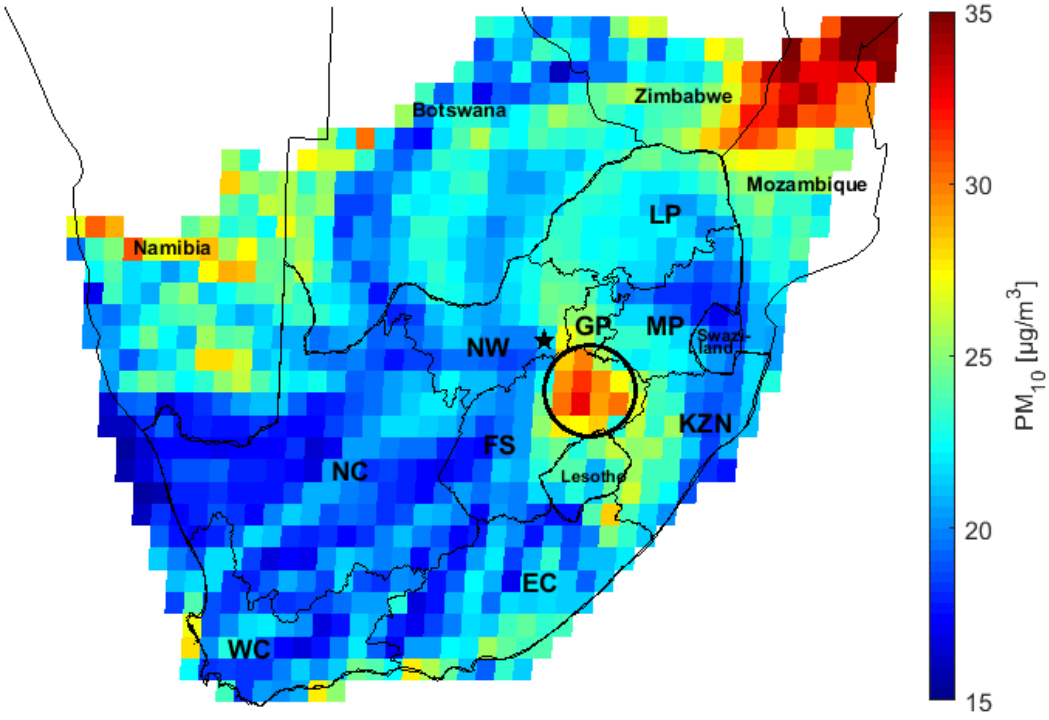

Fig. 6: Auto-generated source map of PM_{10} concentrations observed at Welgegund according to the method by Vakkari et al. (2013, 2011). The circled area indicates the eastern Free State. Province abbreviations: WC – Western Cape, NC – Northern Cape, EC – Eastern Cape, FS – Free State, NW – North West, GP – Gauteng Province, LP – Limpopo Province, MP – Mpumalanga Province, KZN – KwaZulu-Natal.

To further shed light on the sources that influence the aerosol optical properties considered, the method applied to PM_{10} (Fig. 6) was applied for σ_{SP}, σ_{AP}, ω_0 and α_{SP}, measured over the entire sampling period considered, as indicated in Figs. 7a, b, c and d, respectively. Form the results (Fig. 7a and b) high σ_{SP} and σ_{AP} were observed in air masses that had passed over eastern Zimbabwe and central Mozambique. This correlates with the high frequency of open biomass burning (Fig. 2b) observed over these areas. The open biomass burning emissions from eastern Zimbabwe and central Mozambique are expected to be higher per unit surface area due to the more productive savannah vegetation type biome occurring there, if compared to the grassland vegetation type biome that covers a significant portion of the South African interior. Tiitta et al. (2014) proved that OA makes up the largest fractional contribution of PM_1 measured at Welgegund, especially during the dry and open biomass burning season when biogenic volatile organic compound (BVOC) emissions from vegetation are at a minimum (Jaars et al, 2016). Maritz et al. (2020) proved that this is similarly true for $PM_{2.5}$ particulate organic matter (POM) at a number of sites in the South African interior. For σ_{SP} (Fig. 7a), a combination of wind-blown dust originating from the eastern Free State (as indicated earlier, i.e. Fig. 6 and associated discussions) and emissions from the industrialised Vaal Triangle, also lead to elevated values. Additionally, it is evident that source regions that are significantly influenced by anthropogenic activities (e.g. Vaal Triangle, Mpumalanga Highveld, Jhb-Pta megacity) and/or higher open biomass burning (Fig. 2b) and/or higher population density (Fig. 1) had higher σ_{SP} and σ_{AP}, than the relatively clean background in the sector between north northwest and south southwest, to the west of Welgegund. It was also interesting to note that emissions from open biomass burning (Fig. 2b) in northern KwaZulu-Natal and the Eastern Cape areas that border Lesotho contributed to elevated σ_{AP} levels, more so than for σ_{SP}. These areas are located in escarpment regions, which receive very high rainfall and are prone to relatively

high open biomass burning frequencies, as indicated in Fig. 2b. It cannot be speculated from currently available data why open biomass burning in these regions would emit more absorptive (e.g. eBC) than scattering species (e.g. OA), if compared to other regions. However, this should be investigated in more detail in future.

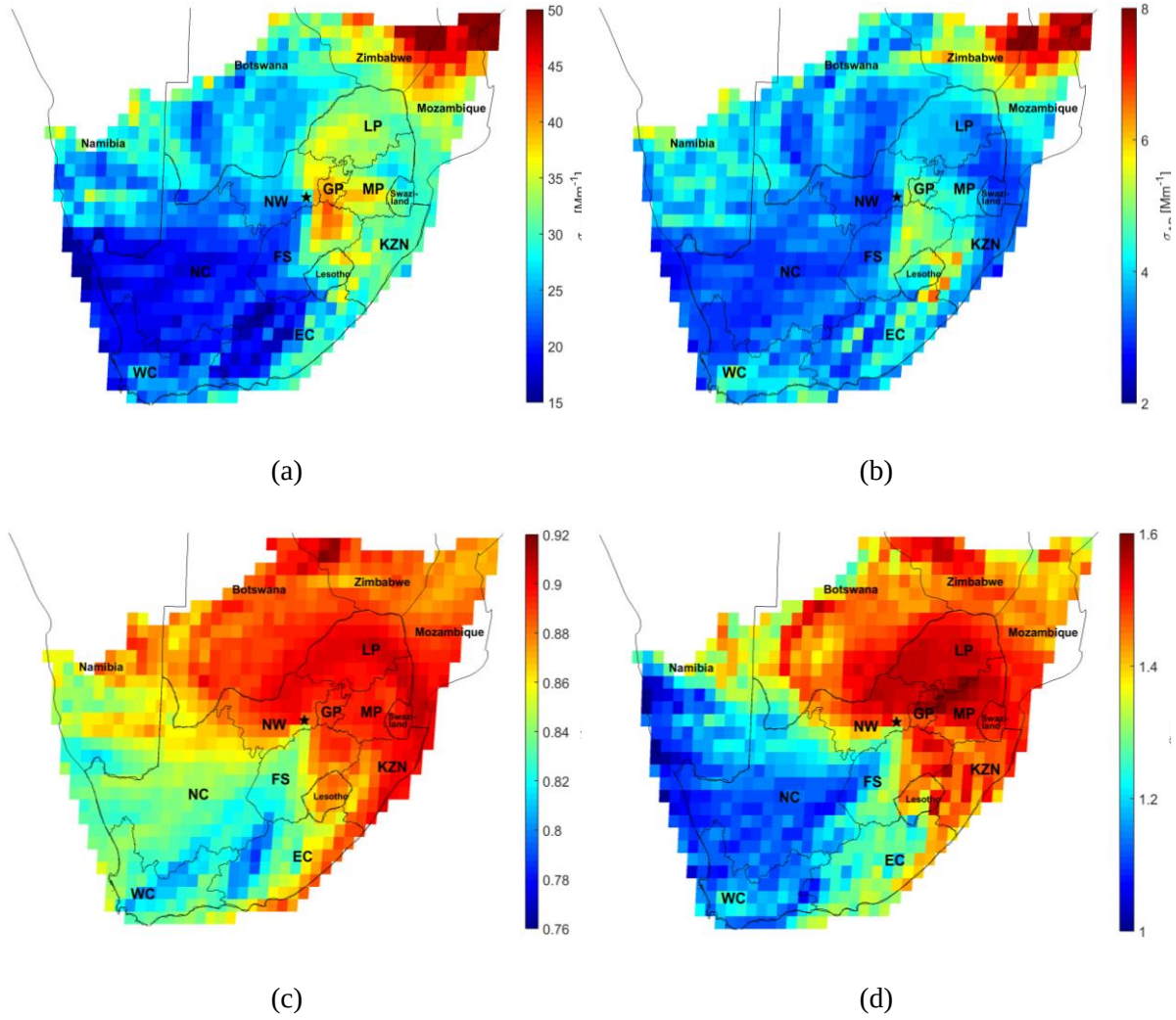

Fig. 7: Auto-generated source maps of the optical properties (a) σ_{SP}, (b) σ_{AP}, (c) ω_0 and (d) α_{SP} observed at Welgegund for the entire sampling period, according to the method introduced by Vakkari et al. (2013, 2011). Province abbreviations: WC – Western Cape, NC – Northern Cape, EC – Eastern Cape, FS – Free State, NW – North West, GP – Gauteng Province, LP – Limpopo Province, MP – Mpumalanga Province, KZN – KwaZulu-Natal.

From Fig. 7c, presenting the ω_0 auto-generated source map, it is clear that more scattering aerosols originate for areas that have higher open biomass burning frequencies (Fig. 2b), higher population densities and higher concentrations of large point sources (Fig. 1). The dominant scattering properties of aerosols from these regions results in higher ω_0, than the ω_0 of air masses that have passed of the sector between west-southwest and south-south of Welgegund. In addition the area over which air masses passed that had the highest ω_0 correspond relatively well with the dominant anti-cyclonic recirculation path of air masses that transport emissions from the industrial hub of South Africa (e.g. as presented in Booyens et al., 2019), which is again evidence of the influence of anthropogenic activities on the aerosol optical properties.

Fig. 7d presents the α_{SP} auto-generated source map for Welgegund. Similar to the deduction made for the ω_0 it is evident from this figure that smaller particles originate from areas that have higher open biomass burning frequencies (Fig. 2b), higher population densities (Fig. 1) and higher concentrations of large point sources (Fig.

1), while larger particles are observed in air masses that have passed of the sector between west-southwest and south-southwest of Welgegund.

From Fig. 7 source deductions could be made that were relevant for the entire sampling period. In order to isolate the influence of the various sources better, source maps (similar to Fig. 7) were drawn of σ_{SP} (Fig. S5), σ_{AP} (Fig. S6), ω_0 (Fig. S7) and α_{SP} (Fig. S8) for three distinct periods, i.e.:

(a) The warmest (Fig. S1a) and wettest (Fig. S1c) period, i.e. December, January and February, when almost no open biomass burning occurred (Fig. 2a) and domestic combustion for space heating was insignificant.

(b) The coldest period i.e. June and July (Fig. S1a), when domestic space heating was most prevalent, while open biomass burning did not yet reach a maximum (Fig. 2a)

(c) The driest period (Fig. S1c) with the highest fire frequencies (Fig. 2a). The latter was defined as 15 August–15 October, since June to approximately 15 August is the coldest period, during which significant contribution from domestic space heating can be expected.

During the warmest/wettest period, the σ_{SP} was highest in air masses that had passed over the Jhb-Pta megacity, the Mpumalanga Highveld and the Vaal Triangle (Fig. S5a), which reflect the contribution of industrial emissions (as previously explained in Section 2). Similar high values were observed for the eastern Free State (Fig. 1), which likely represent the influence of wind-blown dust emanating from agricultural activities (Fig. 6). Slightly lower values, but still elevated, were observed in air masses that followed the typical anti-cyclonic recirculation pattern. During the coldest period (Fig. S5b), the highest σ_{SP} values were observed in air masses that had passed over a similar, but slightly larger area, than observed for the highest σ_{SP} in the warmest/wettest period (Fig. S5a). This extended area reflects the population density, which is highest in the Gauteng Province (Fig. 1). Therefore, although the influence of industrial activities and open biomass combustion could not totally be eliminated by focussing on the coldest period, the afore-mentioned result clearly indicates the regional influence of domestic combustion for space heating. In contrast to the above-mentioned, σ_{SP} was highest in air masses that had passed over the eastern Zimbabwe and central Mozambique during the driest period when open biomass burning peaked (Fig. S5c). Additionally, during the same time the significant contribution of wind-blown dust from the eastern Free State was evident.

The σ_{AP} was the highest in air masses that had passed over the Mpumalanga Highveld, Jhb-Pta megacity and KwaZulu-Natal during the warmest/wettest period (Fig. S6a), indicating the contribution of industrial activities. Higher values for σ_{AP} in air masses that passed over a similar area as the high values observed during the warmest/wettest period can be observed during the coldest period (Fig. S6b). This indicates the contribution of domestic combustion for space heating, as mentioned previously, in addition to the industrial activities identified in Fig. S6a.

It was also very interesting to note that the larger Cape Town area was indicated in Fig. S6b as a potential source of higher σ_{AP} measured at Welgegund during the coldest period. During this time of the year it is well known that cold fronts approach South Africa from the southwest (e.g. Fig. S4, Techcentral, 2019). Therefore, although the auto-generated source map (Fig. S6b) is not conclusive evidence that emissions from the larger Cape Town area contribute to elevated σ_{AP} measured at Welgegund, it supports the notion that it is possible. Additionally, statistically enough trajectories had passed over the larger Cape Town area to enable the auto-generated source map to classify it during the coldest period (Fig. S6b), while this was not the case for the warmest/wettest period (Fig. S6a). Jenner and Abiodun (2013) previously postulated that SO_2 from the

Mpumalanga Highveld can be transported episodically to the Cape Town area, therefore the postulation of pollution transport in the reverse direction during the coldest period by means of cold fronts (associated with relatively fast moving air masses) seem possible. It is also noteworthy to mention that census data indicate a significant population growth for the Cape Town Metropolitan area from 2.56 to 3.74 million inhabitants between 1996 and 2011 (newer data was not available) (StatsSA, 2019). Most of this growth can likely be attributed to increasing population in semi- and informal settlements, wherein domestic combustion for space heating is prevalent. Considering the afore-mentioned, the possible episodically transport of pollution from the larger Cape Town area to the South African interior should be investigated in greater detail in future.

Form Fig. S6c, presenting the driest peak open biomass burning period, it is evident that the highest σ_{AP} values occurred in air masses that had passed over eastern Zimbabwe and central Mozambique These areas were previously identified as having some of the highest open biomass burning frequencies within the spatial area considered (Fig. 2b) . In contrast, the lowest σ_{AP} was observed in air masses that had passed over the sector west to south-west of Welgegund (i.e. regional background), during the same period.

Fig. S7 presents the ω_0 auto-generated source map for the three identified periods. As in all other ω_0 discussions it should be remembered that ω_0 is the net effect of σ_{SP} and σ_{AP}. Therefore, the σ_{SP} and σ_{AP} auto-generated source maps for the three identified periods should be considered to explain the observed ω_0 source maps. As an example, σ_{SP} and σ_{AP} was the highest in air masses that had passed over eastern Zimbabwe and central Mozambique during the driest period (Fig. S5c and S6c), however, in the correlating ω_0 source maps (Fig. S7c) this area had moderate ω_0 values that were lower than the Mpumalanga Highveld. A feature that is common to all the ω_0 auto-generated source maps for the three identified periods is that lower ω_0 values were observed in air masses that had passed over the sector between west-southwest and south-southwest of Welgegund. In contrast, higher ω_0 values were observed in air masses that had passed over areas that have higher open biomass burning frequencies (Fig. 2b), higher population densities (Fig. 1) and higher concentration of large point sources (Fig. 1).

As was the case for so many of the previous auto-generated source maps, the α_{SP} values observed in air masses that had passed over the sector between west-southwest and south-southwest of Welgegund were lower (implying larger particles, generally associated with natural sources such as wind-blown dust) for all the three identified periods (Fig. S8a, b and c). In contrast, higher α_{SP} values (implying smaller particles) were observed in air masses that had passed over areas that have higher open biomass burning frequencies (Fig. 2b), higher population densities (Fig. 1) and higher concentrations of large point sources (Fig. 1).

An interesting feature of the α_{SP} source map for the wettest/warmest period (Fig. S8a) is that elevated α_{SP} values (i.e. smaller particles) were observed in air masses that had passed over eastern Botswana. Although a similar feature was not the most obvious feature in the corresponding σ_{SP} auto-generated source map (Fig. S5a) it was evident. The only possible explanation for this feature, i.e. increase small particles that are more scattering during the warmest/wettest period, is biogenic emissions from this part of the savannah vegetation type biome that are converted to OA. The reason(s) why this specific part of the savannah vegetation type biome is different could not be explained, but should be investigated in future studies.

For the coldest period (Fig. S8b) higher α_{SP} values were evident over the entire Gauteng province (highest population density, Fig. 1), if compared with the other two periods (Fig. S8a and c). This indicates the effect of domestic combustion for space heating. Similar to what was observed during the coldest period for σ_{AP} (Fig. S6b), evidence for possible transport of aerosol pollution from the Western Cape is also observed in Fig. S8b.

In addition to the specific observations presented for σ_{SP} (Fig. S5), σ_{AP} (Fig. S6), ω_0 (Fig. S7) and α_{SP} (Fig. S8) for the three distinct periods, three common features can be identified from the afore-mentioned figures. Firstly, much lower emissions are evident in the sector between north and south-west of Welgegund (i.e. the regional background), which can be subdivided into two regions, i.e. the Kalahari (north to west of Welgegund) and Karoo (west to south-west of Welgegund). For the latter, emission in the Karoo seems lower than that observed for the Kalahari. Secondly, the influence of the anti-cyclonic recirculation pattern, which recirculates the emissions from north-eastern South Africa, is apparent. Thirdly, higher emissions (related to industries/population density/fire frequency) are associated with north-eastern South Africa. Considering the afore-mentioned features, air masses sampled at Welgegund were further classified as passing over these four defined regions (i.e. Karoo, Kalahari, anti-cyclonic recirculation pattern and industrial hub), as presented in Fig. 8.

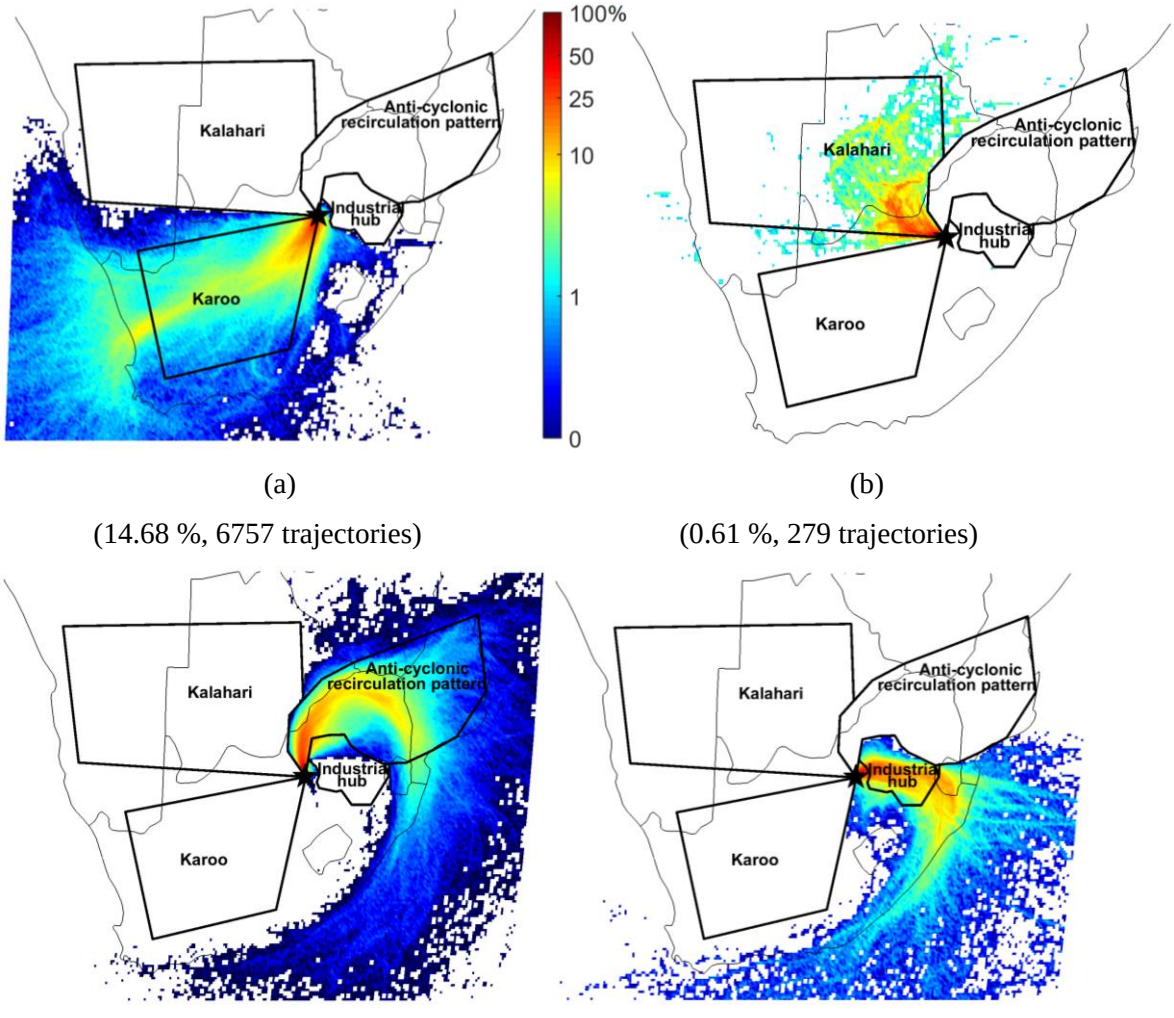

Fig. 8: Overlay back trajectory maps (Section 3.3), for the entire sampling period, allocated as passing (spending at least 10 hours) over the (a) Karoo region, (b) Kalahari region, (c) anti-cyclonic recirculation pattern and (d) industrial hub before being sampled at Welgegund. The colour code indicates the percentage of trajectories passing over each grid cell, with dark blue and red indicating the lowest and highest number of trajectory overpasses, respectively. The percentage values indicated in brackets below each figure indicates what percentage of the overall trajectories could be classified as passing over a specific region, with the actual number of hourly arriving trajectories that this represent next to it.

Fig. 9 presents the statistical distribution of the aerosol optical properties classified according to air masses that had passed over the four defined regions (Fig. 8) during the three distinct time periods specified, i.e. (i) the warmest/wettest, (ii) coldest and (iii) driest, and peak open biomass burning periods.

From Fig. 9a it is evident that the σ_{SP} medians observed for air masses that had passed over the Karoo (6.3 M m^{-1}) and Kalahari (8.3 M m^{-1}) during the warmest/wettest period were similar, while the corresponding medians observed for air masses that had passed over the anti-cyclonic recirculation pattern (20.9 M m^{-1}) and industrial hub (22.5 M m^{-1}) were similar. The σ_{SP} median for the Karoo was approximately 72 % lower than that observed for the industrial hub. During this period (warmest/wettest) low fire frequencies occur (Fig. 2a). Therefore, this significant difference between the Karoo and industrial hub (72 % in median σ_{SP}) indicates the dissimilarities between to the two regions in anthrophonic activities (e.g. industrial, traffic, domestic cooking) and vegetation type biome productivity, which is associated with open biomass burning frequencies. Similar observations are evident from Fig. 9b, for the σ_{AP} medians during the warmest/wettest period. During this time period σ_{AP} median for air masses that had passed over the Kalahari (0.7 M m^{-1}), which were slightly lower than that of the Karoo (1.0 M m^{-1}), was approximately 71 % lower than σ_{AP} median of air masses passing over the industrial hub (2.3 M m^{-1}).

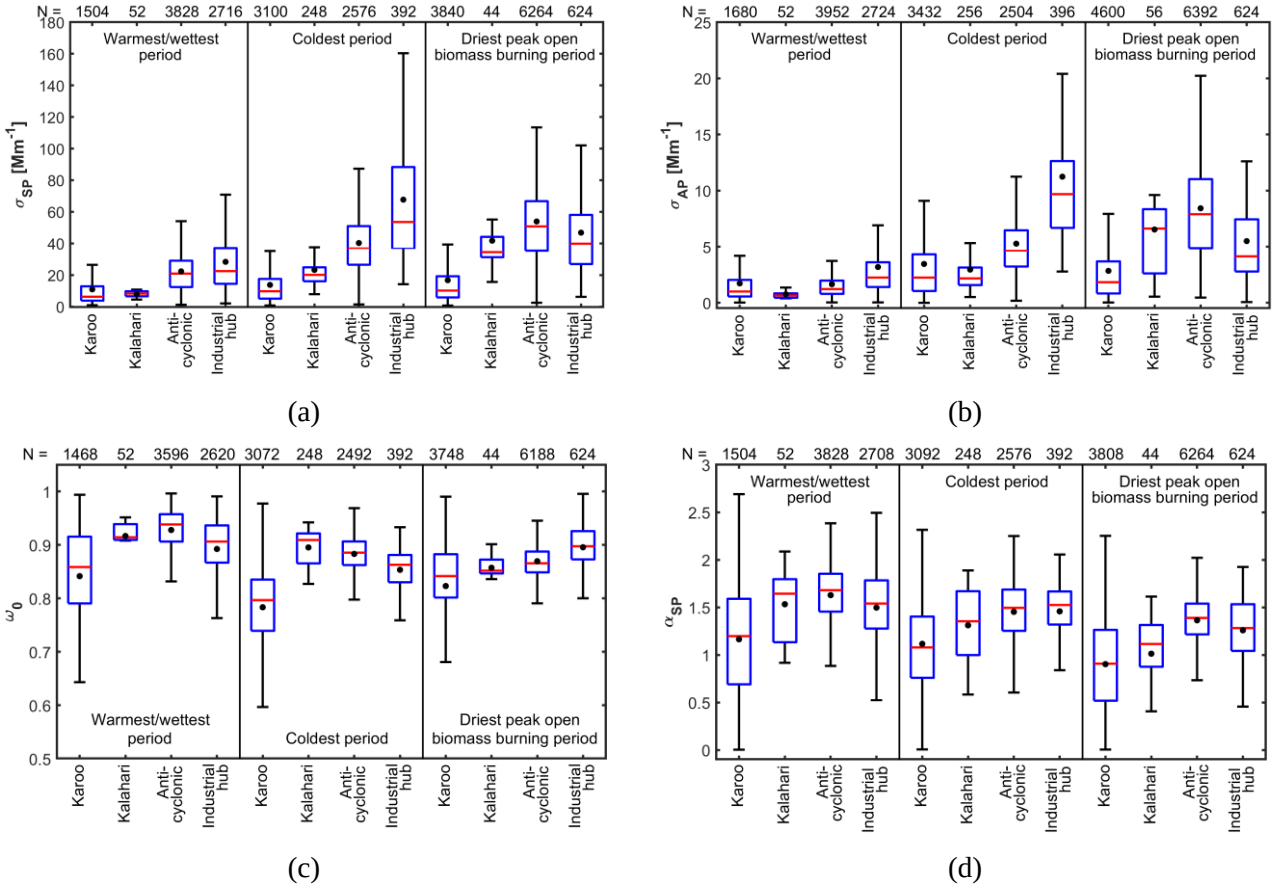

Fig. 9: Statistical distribution of the (a) σ_{SP}, (b) σ_{AP}, (c) ω_0 and (d) α_{SP} based on air masses that had passed over the Karoo region, Kalahari region, the anti-cyclonic recirculation pattern and the industrial hub classified according to warmest/wettest, coldest, and driest and peak open biomass burning periods. The red line represents the median, the black dot the mean, the top and bottom edges of blue boxes the 25 and 75 % percentile and the black whiskers indicates a 99.3 % coverage. The number (N) of 15 min data points represented by each box and whisker is indicated at the top of each graph.

During the coldest period (Fig. 9a) air masses that had passed over the industrial hub had the highest σ_{SP} median (53.6 M m^{-1}). This was approximately 82 % higher than the σ_{SP} median observed for air masses that had

passed over the Karoo (9.7 M m^{-1}), which had the lowest median. Since open biomass burning frequencies do not yet peak during the coldest period (Fig. 2a), the difference between the afore-mentioned medians reflect the dissimilarity in contribution to σ_{SP} from domestic combustion for space heating, in addition to sources that contribute year round (e.g. industry, traffic and domestic cooking) between the two regions. Similar observations are evident from Fig. 9b, for the σ_{AP} medians during the coldest period. During this time period σ_{AP} medians for air masses that had passed over the Karoo (2.3 M m^{-1}) and Kalahari (2.2 M m^{-1}) were similar. These medians were approximately 77 to 78 % lower than σ_{AP} median of air masses passing over the industrial hub (9.7 M m^{-1}).

The σ_{SP} median for air masses that had passed over the Karoo (10.1 M m^{-1}) during the driest, peak open biomass burning period was approximately 80 % lower than the median observed for air masses that had passed over the anti-cyclonic recirculation pattern (50.8 M m^{-1}). In contrast to the previous periods, σ_{SP} median of the anti-cyclonic recirculation pattern was higher than that of the industrial hub (39.8 M m^{-1}), due to the former region being covered mostly by the more productive (biomass per surface unit) savannah vegetation type biome, while the latter region is covered by a combination of grassland and savannah vegetation type biomes (Fig. 1). The difference between the σ_{SP} medians of the Karoo and the anti-cyclonic recirculation pattern during the driest, peak open biomass burning period therefore reflect the dissimilar contributions of the open biomass burning emissions between the two regions. Similar observations are evident from Fig. 9b, for the σ_{AP} medians during the driest, peak open biomass burning period. During this time, air masses that had passed over the Karoo (1.8 M m^{-1}) had a σ_{AP} median of approximately 77 % lower than air masses that had passed over the anti-cyclonic recirculation pattern (7.9 M m^{-1}).

By considering Fig. 9c it is evident that the ω_0 medians of air masses that had passed over the Karoo (varying between 0.80–0.86) during all the isolated periods (i.e. warmest/wettest; coldest; and driest, peak open biomass burning) were lower than the corresponding medians of the Kalahari (varying between 0.85–0.91), anti-cyclonic recirculation pattern (varying between 0.87–94) and industrial hub (varying between 0.86–0.91). For the different time periods, the Karoo ω_0 medians were 9, 12 and 7 % lower than the area with the highest ω_0 median, in the warmest/wettest, coldest, and driest, peak open biomass burning periods, respectively. The difference between the ω_0 medians of the Karoo and the other regions reflect the dissimilar contributions of anthropogenic, open biomass burning and biogenic emissions between the Karoo and the other regions during the different time periods.

In a similar manner α_{SP} medians (Fig. 9d) of the Karoo (varying between 0.91–1.20) were smaller than the corresponding α_{SP} medians of the Kalahari (varying between 1.12–1.62), anti-cyclonic recirculation pattern (varying between 1.50–1.68) and the industrial hub (varying between 1.28–1.54) during all the considered time periods. For the different time periods, the Karoo α_{SP} medians were 29, 29 and 35 % lower than the anti-cyclonic recirculation pattern, which had the highest α_{SP} medians, in the warmest/wettest, coldest, and driest, peak open biomass burning periods, respectively. The afore-mentioned prove that larger particles are typically observed in air masses that had passed over the Karoo, if compared to air masses that had passed over the other defined regions. As previously stated, larger particles are typically associated with natural processes (e.g. wind-blown dust), while finer particles are typically associated with anthropogenic activities and/or biomass burning. Also, the longer aging time of anthropogenic gaseous pollutants present in air masses that had passed over the anti-cyclonic recirculation pattern results in a larger fraction contribution from secondary aerosols, which are smaller than primary particles.

4.5 Contextualisation of aerosol optical properties

In Table 1, the mean aerosol optical properties for the entire sampling period, for the different periods (i.e. (i) warmest/wettest, (ii) coldest and (iii) driest, peak biomass burning periods), and the defined regions (i.e. Karoo, Kalahari, anti-cyclonic recirculation pattern and industrial hub), measured at Welgegund are presented. Some of these values are compared with mean or median optical properties measured at other sites, which are presented in Table 2, to contextualise the Welgegund aerosol optical properties.

During the warmest/wettest, coldest, as well as driest, peak open biomass burning periods the σ_{SP} means for air masses that had passed over the Karoo were 6.3, 9.7 and 10.1 M m^{-1}, respectively, which are comparable to σ_{SP} means reported for true background sites such as Barrow Alaska, USA (10.4 M m^{-1}) (Delene and Ogren, 2002), Pallas-Sodankylä, Finland (4.9 M m^{-1}) (Lihavainen et al., 2015) and Andøya Island, Norway (5.4 M m^{-1}) (Montilla et al., 2011). The highest σ_{SP} mean for all defined source areas over all the investigated time periods were observed in air masses that had passed over the industrial hub during the coldest period, which had a median of 53.6 M m^{-1}. This compares to the σ_{SP} mean reported for Elandsfontein (South Africa) (49.5 M m^{-1}), but it is significantly lower than σ_{SP} means reported for polluted sites in China (ranging between 158 to 488 Mm^{-1}) (Cheng et al., 2008; Yan et al., 2008; Xu et al., 2004; Xu et al., 2002; Bergin et al., 2001).

The σ_{AP} means for all the defined source regions and during all the considered time periods were higher than σ_{AP} means reported for true background sites such as Barrow Alaska, USA (0.4 M m^{-1}) (Delene and Ogren, 2002), Pallas-Sodankylä, Finland (0.6 Mm^{-1}) (Lihavainen et al., 2015) and Andøya Island, Norway (0.4 Mm^{-1}) (Montilla et al., 2011). The lowest σ_{AP} means observed were during the warmest/wettest period for air masses that had passed over the Karoo (1.0 M m^{-1}) and Kalahari (0.7 M m^{-1}). The highest σ_{AP} mean observed was for the industrial hub during the coldest period (9.7 M m^{-1}), which was similar to the σ_{AP} mean reported for Elandsfontein, South Africa (8.3 M m^{-1}, Laakso et al., 2012), but substantially lower than σ_{AP} means reported for polluted sites in China (ranging between 17.5–83.0 Mm^{-1}) (Cheng et al., 2008; Yan et al., 2008; Xu et al., 2002; Xu et al., 2004; Bergin et al., 2001).

The ω_0 means of air masses that have passed over the Karoo were substantially lower than ω_0 means of air masses that had passed over the other defined regions during all the considered time periods. The ω_0 means observed for the Karoo (0.80–0.86) were lower (more absorbing) than true background sites such as Barrow Alaska, USA (0.96) (Delene and Ogren, 2002), Pallas-Sodankylä, Finland (0.90) (Lihavainen et al., 2015) and Andøya Island, Norway (0.91) (Montilla et al., 2011). ω_0 means for polluted sites in China have been reported to vary between 0.81–0.95 (Cheng et al., 2008; Yan et al., 2008; Xu et al., 2002; Xu et al., 2004; Bergin et al., 2001). However, since the climatological effect of ω_0 also depends on the albedo of the underlying surface (e.g. Haywood and Boucher, 2000; Haywood and Shine, 1995) it is not that straight forward to directly compare the ω_0 of different sites. For example, for a typical 0.2 surface reflectance of grass, aerosols may heat the atmosphere if the ω_0 is less than 0.75 and *vice versa* for cooling (e.g. Betts and Ball, 1997). Considering the latter grassland values, it implies that in general aerosols at Welgegund have a net cooling effect, which makes sense, considering it is a site for which the aerosol composition is dominated by scattering species, e.g. OA and SO_4^{2-} (Venter et al., 2018; Aurela et al., 2016; Tiitta et al., 2014).

During all the considered time periods, the α_{SP} means for air masses that had passed over the Karoo (0.9–1.2) were equal and lower (larger particles) than α_{SP} means reported for true background sites such as Barrow Alaska, USA (1.2) (Delene and Ogren, 2002), Pallas-Sodankylä, Finland (1.7) (Lihavainen et al., 2015) and Andøya

Island, Norway (1.4) (Montilla et al., 2011), and higher than α_{SP} means reported for sites that are directly impacted mainly by wind-blown dust, e.g. Cape Verde (0.36) and Solar village, Saudi Arabia (0.41) (Dubovik et al., 2001). The highest α_{SP} mean was observed for air masses that had passed over the anti-cyclonic recirculation pattern (1.68) during the warmest/wettest period, which was lower than α_{SP} medians reported for sites that are directly impacted by anthropogenic activities (smaller particles) such as Bondville, Illinois, USA (2.0) (Delene and Ogren, 2002), Paris, France (1.8) and Mexico City, Mexico (1.8) (Dubovik et al., 2001).

Table 1: Mean aerosol optical properties measured at Welgegund for the entire sampling period and for the different periods (warmest/wettest, coldest and, driest, peak open biomass burning) over the defined source regions (Karoo, Kalahari, anti-cyclonic recirculation pattern, industrial hub).

Welgegund

Different periods	Defined region	σ_{SP} (M m^{-1})	σ_{AP} (M m^{-1})	ω_0	α_{SP}
Entire sampling period	All regions	23.77	2.36	0.89	1.52
Warmest/wettest	Karoo	6.27	1.01	0.86	1.20
	Kalahari	8.25	0.66	0.91	1.64
	Anti-cyclonic recirculation pattern	20.90	1.22	0.94	1.68
	Industrial hub	22.47	2.25	0.91	1.54
Coldest	Karoo	9.72	2.25	0.80	1.08
	Kalahari	20.10	2.18	0.91	1.35
	Anti-cyclonic recirculation pattern	36.74	4.67	0.89	1.50
	Industrial hub	53.56	9.69	0.86	1.53
Driest, peak open biomass burning	Karoo	10.12	1.84	0.84	0.91
	Kalahari	34.49	6.62	0.85	1.12
	Anti-cyclonic recirculation pattern	50.76	7.9	0.87	1.39
	Industrial hub	39.81	4.14	0.90	1.28

Table 2: The mean aerosol optical properties measured at other sites. Only the Skukuza (South Africa) and Mongu (Zambia) values were reported as medians.

Other sites

Sites	σ_{SP} (M m^{-1})	σ_{AP} (M m^{-1})	ω_0	α_{SP}	Sites	σ_{SP} (M m^{-1})	σ_{AP} (M m^{-1})	ω_0	α_{SP}
Bondville, Illinios (USA) (Delene and Ogren, 2002)	57.00	4.62	4.62	2.03	Yulin (China) (Xu et al., 2004)	158.00	6.00	0.95	
Sable Island, Nova Scotia (Canada) (Delene and Ogren, 2002)	40.70	1.89	1.89	0.83	Beijing (China) (Bergin et al., 2001)	488.00	83	0.81	
Barrow, Alaska (Canada) (Delene and Ogren, 2002)	10.40	0.38	0.38	1.20	Goddard Space Flight Center Greenbelt (USA) (Dubovik et al., 2001)			0.97	1.90
Lamont, Oklahoma (USA) (Delene and Ogren, 2002)	46.7	2.47	2.47	1.90	Paris (France) (Dubovik et al., 2001)			0.93	1.80
Pallas-Sodankylä, (Finland) (Aaltonen et al., 2006)	4.60			1.80	Mexico City (Mexico) (Dubovik et al., 2001)			0.88	1.80
Pallas-Sodankylä, (Finland) (Lihavainen et al., 2015)	4.90	0.57	0.57	1.70	Maldives (Dubovik et al., 2001)			0.89	1.55
Elandsfontein (SA) (Laakso et al., 2012)	49.50	8.30	8.30	1.50	Amazonian forest Brazil and Bolivia (Dubovik et al., 2001)			0.93	1.95
Mace head (Ireland) (Kleefeld et al., 2002)	20.80				Cerrado Brazil (Dubovik et al., 2001)			0.89	1.85
Cape grim, (Tasmania) (Carrico et al., 1998)	15.40				Zambia (Dubovik et al., 2001)			0.84	1.95
Mace head (Ireland) (Marine)		0.31	0.31		Canada (Dubovik et al., 2001)			0.94	1.96

(Junker et al., 2006)							
Mace head (Ireland) (Continental) (Junker et al., 2006)		3.93	3.93		Bahrain/Persian Gulf (Dubovik et al., 2001)	0.95	1.10
AndØya Island, (Norway) (Montilla et al., 2011)	5.42	0.40	0.40	1.37	Solar-village (Saudi Arabia) (Dubovik et al., 2001)	0.96	0.41
Skukuza (SA) (Queface et al., 2011)				1.41	Cape Verde (Dubovik et al., 2001)	0.98	0.36
Mongu (Zambia) (Queface et al., 2011)				1.73	Lanai (Hawaii) (Dubovik et al., 2001)	0.97	1.40
Xianghe (China) (Li et al., 2008)					Alta Floresta Brazil (Reid et al., 1999)	0.86	0.97
Xinken (China) (Cheng et al., 2008)	333.00	61.00	61.00	1.60	Cuiaba Brazil (Reid et al., 1999)	0.85	1.08
Shangdianzi (China) (Yan et al., 2008)	174.60	17.54	0.88		Ji Parana Brazil (Reid et al., 1999)	0.87	0.82
Lin'an (China) (Xu et al., 2002)	353.00	23.00	0.93				

5 Summary and conclusions

This paper reports the longest continuous, *in situ*, ground level scattering and absorption dataset for the South African interior, published in the peer reviewed public domain. Measurement were conducted at a strategically position site that allowed differentiation of the impact of anthropogenic activities, population density, difference in vegetation type biomes and open biomass burning frequency on the aerosol optical properties.

σ_{SP} and σ_{AP} were generally higher in winter and early spring, and lower in summer and autumn. For ω_0, lower values were observed in winter and early spring, and higher values in summer and early autumn. The ω_0 diurnal pattern indicated more scattering species during daytime. All these temporal patterns were explained by considering southern African specific sources and metrological conditions.

Auto-generated source maps gave insight on the spatial importance of source regions. Air masses that had passed over source regions i) significantly influenced by industrial and anthropogenic activities (e.g. Vaal Triangle, Mpumalanga Highveld, Jhb-Pta megacity), ii) where over emission from the afore-mentioned areas were circulated, iii) that had higher open biomass burning frequency and iv) with higher population density, had higher σ_{SP}, σ_{AP} and ω_0, and lower α_{SP}, if compared with the relatively clean background. Auto-generated source maps of the a) warmest/wettest, b) coldest, and c) driest and peak open biomass burning periods allowed the influence of the different sources to be better isolated. The influence of anthropogenic activities in the Jhb-Pta megacity, the Mpumalanga Highveld and Vaal Triangle were isolated in the warmest/wettest period. During the coldest period, the same source regions (as in warmest/wettest period), but with a slightly larger footprint, as well as higher σ_{SP}, σ_{AP} and $\omega_{0,}$ and lower α_{SP}, were evident, which proved the regional impact of household space heating. During the driest and peak open biomass burning period, the influence of more open biomass burning to the east and less to the west of Welgegund was evident. Additionally, eastern Zimbabwe and central Mozambique were identified as significant source regions.

To quantify differences indicated by the auto-generated source maps, four source regions were defined, i.e. Karoo, Kalahari, anti-cyclonic recirculation pattern and the industrial hub. From the results it was evident that air masses that had passed over the Karoo source region represented the most natural background, while air masses

that had passed over the anti-cyclonic recirculation pattern and the industrial hub were significantly influenced by anthropogenic activities.

Acknowledgements

This publication forms part of the output of the Biogeochemistry Research Infrastructure Platform (BIOGRIP) of the Department of Science and Innovation of South Africa.

Data statement

Collaboration is welcomed and data used in this study can be requested from paul.beukes@nwu.ac.za (J.P Beukes), pieter.vanzyl@nwu.ac.za (P.G. Van Zyl) or ville.vakkari@fmi.fi (V. Vakkari).

References

Aaltonen, V., Lihavainen, H., Kerminen, V.-M., Komppula, M., Hatakka, J., Eneroth, K., Kulmala, M., and Viisanen, Y.: Measurements of optical properties of atmospheric aerosols in Northern Finland, Atmos. Chem. Phys., 6, 1155–1164, https://doi.org/10.5194/acp-6-1155-2006, 2006

Ångström, A.: On the atmospheric transmission of sun radiation and on dust in the air, Geogr. Ann. A., 156–166, https://doi.org/10.2307/519399, 1929

Archibald, S., Roy, D.P., Van Wilgen, B.W., Scholes, R.J.: What limits rire? An examination of driver's of burnt area in southern Africa. Global Change Biology (2008). https://doi.org/10.1111/j.1365-2486.2008.01754.x

Aurela, M., Beukes, J.P., Van Zyl, P.G., Vakkari, V., Teinilä, K., Saarikoskii, S., and Laakso, L.: The composition of ambient and fresh biomass burning aerosols at a savannah site, South Africa, S. Afr J. Sci., 112, 1–8, https://doi.org/10.17159/sajs.2016/20150223, 2016

Barnard, P.: Biological diversity in Namibia: a clash of sea and land, fog and dust, Biodiversity and Conservation, 7, 415–417, https://doi.org/10.1023/A:1008840031391, 1998

Bergin, M., Cass, G.R., Xu, J., Fang, F., Zeng, L.M., Yu, T., Salmon, L.G., Kiang, C.S., Tang, X.Y., Zhang, Y.H., and Chameides, W.L.: Aerosol radiative, physical, and chemical properties in Beijing during June 1999, J. Geophys. Res.-Atmos., 106, 17969–17980, https://doi.org/10.1029/2001JD900073, 2001

Betts, A.K. and Ball, J.H.: Albedo over the boreal forest. J. Geophys. Res., 102, 28901–28909, https://doi.org/10.1029/96JD03876, 1997

Beukes, J.P, Van Zyl, P.G., Venter, A.D., Josipovic, M., Jaars, K., Tiitta, P., Pienaar, J.J., Laakso, L., Vakkari, V., Kulmala, M., and Worsnop, D.: Source region plume characterisation of the interior of South Africa as observed at Welgegund, Clean Air Journal, 23, 7–10, 2013

Beukes, J.P., Venter, A.D., Josipovic, M., Van Zyl, P.G., Vakkari, V., Jaars, K., Dunn, M. and Laakso, L.: Chapter 6: Automated continuous air monitoring, in: Comprehensive Analytical Chemistry: Monitoring of air pollutants – Samling, sample, preparation and analytical techniques, edited by: Forbes, P., Elsevier, Kidlington, Oxford, UK, Waltham, MA, USA, 183–206, 2015

Booyens, W., Van Zyl, P.G., Beukes, J.P., Ruiz-Jimenez, J., Kopperi, M., Riekkola, M.-L., Josipovic, M., Venter, A.D., Jaars, K. and Laakso, L.: Size-resolved characterisation of organic compounds in atmospheric aerosols collected at Welgegund, South Africa, J. Atmos. Chem., 72, 43–64, https://doi.org/10.1007/s10874-015-9304-6, 2015

Booyens, W., Beukes, J.P., Van Zyl, P.G., Ruiz-Jimenez. J., Kopperi, M., Riekkola, M-L., Josipovic, M., Vakkari, V., and Laakso, L.: Assessment of polar organic aerosols at a regional background site in southern Africa, J. Atmos. Chem., 76, 89–113, https://doi.org/10.1007/s10874-019-09389-y, 2019

Boschetti, L., Roy, D., Hoffmann, A.A.: MODIS Collection 5 Burned Area Product - MCD45. User's Guide Version 2.0, 2009

Boschetti, L., Roy, D., Hoffmann, A.A., Humber, M.: MODIS Collection 5.1 Burned Area Product - MCD45. User's Guide Version 3.0.1, 2013

Boucher, O., Randall, D., Artaxo, P., Bretherton, G., Feingold, P., Forster, P., Kerminen, V.-M., Kondo, Y., Liao, H., Lohmann, U., Rasch, P., Satheesh, S.K., Sherwood, S., Stevens, B. and Zhang, X.Y.: Clouds and Aerosols, in: Climate Change 2013: The Physical Science Basis, edited by Stocker, T. F, Qin, D., Plattner, G.–K., Tignor,

M.M.B., Allen, S.K., Boschung, J., Nauels, A., Xia, Y., Bex, V., and Midgley, P.M. Cambridge, U.K., and New York, U.S.A, 571–657, 2013

Bryant, R.G.: Monitoring hydrological controls on dust emissions: preliminary observations from Etosha Pan, Namibia, Geophys. J., 169, 131–141, https://doi.org/10.1111/1475-4959.04977, 2003

Campbell, J.R., Welton, E.J., Spinhirne, J.D., Ji, Q., Tsay, S., Piketh, S.J., Barenburg, M., and Holben, B.N.: Micropulse lidar observations of tropospheric aerosols over northeastern South Africa during the ARREX and SAFARI 2000 dry season experiments, J. Geophys. Res.-Atmos., 108, 8497, https://doi.org/10.1029/2002JD002563, 2003

Carrico, C.M., Rood, M.J., and Ogren, J.A.: Aerosol light scattering properties at Cape Grim, Tasmania, during the first aerosol characterization experiment (ACE 1). J. Geophys. Res.-Atmos., 103, 16565–16574, https://doi.org/10.1029/98JD00685, 1998

Census 2011a: http://www.statssa.gov.za/census/census_2011/census_products/Census_2011_Census_in_brief.pdf (2011a). Accessed 18 November 2019

CIESIN (Center for International Earth Science Information Network), Columbia University, United Nations Food and Agriculture Programme (FAO), and Centro Internacional de Agricultura Tropical (CIAT), 2005, Gridded Population of the World: Future Estimates (GPWFE), Palisades, NY: Socioeconomic Data and Applications Center (SEDAC), Columbia University, http://sedac.ciesin.columbia.edu/gpw, accessed 15 August 2019

Cheng, Y.F., Wiedensohler, A., Eichler, H., Su, H., Gnauk, T., Brüggemann, E., Herrmann, H., Heintzenberg, J., Slanina, J., Tuch, T., Hu, M., and Zhang, Y.H.: Aerosol optical properties and related chemical apportionment at Xinken in Pearl River Delta of China. Atmos. Environ., 42, 6351–6372, https://doi.org/10.1016/j.atmosenv.2008.02.034, 2008

Chiloane, K.E., Beukes, J.P., Van Zyl, P.G., Maritz, P., Vakkari, V., Josipovic, M., Venter, A.D., Jaars, K., Tiitta, P., Kulmala, M., Wiedensohler, A., Liousse, C., Mkhatshwa, G.V., Ramandh, A., and Laakso, L.: Spatial, temporal and source contribution assessments of black carbon over the northern interior of South Africa, Atmos. Chem. Phys., 17, 6177–6196, https://doi.org/10.5194/acp-17-6177-2017, 2017

Collet, K. S., Piketh, S., and Ross, K.,E.: An assessment of the atmospheric nitrogen budget on the South African Highveld, S. Afr J. Sci., 106, 1–9, https://doi.org/10.4102/sajs.v106i5/6.220, 2010

Conradie, E.H., Van Zyl, P.G., Pienaar, J.J., Beukes, J.P., Galy-Lacaux, C., Venter, A.D., and Mkhatshwa, G.V.: The chemical composition and fluxes of atmospheric wet deposition at four sites in South Africa. Atmos. Environ., 146, 113–131, https://doi.org/10.1016/j.atmosenv.2016.07.033, 2016

Delene, D.J. and Ogren, J.A.: Variability of aerosol optical properties at four North American surface monitoring sites, J. Atmos. Sci., 59, 1135–1150. https://doi.org/10.1175/1520-0469(2002)059<1135:VOAOPA>2.0.CO;2, 2002

DAFF (Department: Agriculture, Forestry and Fisheries): https://www.daff.gov.za, accessed 7 June 2017

Diner, D.J., Abdou, W.A., Bruegge, C.J., Conel, J.E., Crean, K.A., Gaitley, B.J., Helmlinger, M.C., Kahn, R.A., Martonchik, J.V., Pilorz, S.H., and Holben, B.N.: MISR aerosol optical depth retrievals over southern Africa during the SAFARI-2000 Dry Season Campaign, Geophys. Res. Lett., 28, 3127–3130, https://doi.org/10.1029/2001GL013188, 2001

Draxler, R.R. and Hess, G.D.: Description of the HYSPLIT 4 Modelling System. NOAA Technical Memorandum ERL ARL–224, 2004

Droughtsa: http://www.droughtsa.org.za/about-the-drought/rainfall-data.html, accessed 5 August 2019

Dubovik., O., Holben, B.N., Eck, T.F., Smirnov, A., Kaufman, Y.J., King, M.D., Tanré, D., and Slutsker, I.: Variability of absorption and optical properties of key aerosol types observed in worldwide locations, J. Atmos. Sci., 59, 590–608, https://doi.org/10.1175/1520-0469(2002)059<0590:VOAAOP>2.0CO;2, 2001

Eck, T., Holben, B.N., Reid, J., Dubovik, O., Smirnov, A., O'neill, N., Slutsker, I., and Kinne, S.: Wavelength dependence of the optical depth of biomass burning, urban, and desert dust aerosols, Journal of Geophysical Research, 104, 31333– 31349, https://doi.org/10.1029/1999JD900923, 1999

Eck, T., Holben, B., Ward, D., Mukelabai, M., Dubovik, O., Smirnov, A., Schafer, J., Hsu, N., Piketh, S., and Queface, A.: Variability of biomass burning aerosol optical characteristics in southern Africa during the SAFARI 2000 dry season campaign and a comparison of single scattering albedo estimates from radiometric measurements, J. Geophys. Res.-Atmos., 108, https://doi.org/10.1029/2002JD002321, 2003

ESKOM: http://www.eskom.co.za/sites/heritage/Pages/Duvha.aspx, accessed 5 August 2019

ESKOM: http://www.eskom.co.za/sites/heritage/Pages/MATLAPOWERSTATION.aspx, accessed 5 August 2019

Formenti, P., Winkler, H., Fourie, P., Piketh, S., Makgopa, B., Helas, G., Andreae, M.O.: Aerosol optical depth over a remote semi-arid region of South Africa from spectral measurements of the daytime solar extinction and the nighttime stellar extinction, Atmos. Res., 62, 11–32, https://doi.org/10.1016/S0169-8095(02)00021-2, 2002

Forster, P., Ramaswamy, V., Artaxo, T., Berntsen, T., Betts, R., Fahey, D.W., Haywood, J., Lean, J., D.C, L., Myhre, G., Nganga, J., Tprinn, R., Raga, G., Schulz, M., and Van Dorland, R.: Changes in atmospheric constituents and in radiative forcing, in: Climate Change 2007: The Physical Science Basis, editied by: Solomon, S., Qin, D., Manning, M., Chen, Z., Marquis, M., Averyt, K.B., Tignor, M. and Miller, H.L, Cambridge, UK and New York, USA, 129–234, 2007

Garland, R. M., Yang, H., Schmid, O., Rose, D., Nowak, A., Achtert, P., Wiedensohler, A., Takegawa, N., Kita, K., Miyazaki, Y., Kondo, Y., Hu, M., Shao, M., Zeng, L.M., Zhang, Y.H., Andreae, M.O., and Pöschl, U.: Aerosol optical properties in a rural environment near the mega-city Guangzhou, China: implications for regional air pollution, radiative forcing and remote sensing, Atmos. Chem. Phys., 8, 5161–5186, https://doi.org/10.5194/acp-8- 5161-2008, 2008

Garstang, M., Tyson, M., Swap, R., Edwards, M., Kållberg, P., and Lindesay, J.A.:. Horizontal and vertical transport of air over southern Africa, J. Geophys. Res., 101, 23721–23736, https://doi.org/10.1029/95JD00844, 1996

GDAS: ftp://arlftp.arlhq.noaa.gov/pub/archives/gdas1/, accessed 15 August 2019

Gierens, R., Laakso, L., Mogensen, D., Vakkari, V., Beukes, J.P., Van Zyl, P.G., Hakola, H., Guenther, A., Pienaar, J.J. and Boy, M.: Modelling new particle formation events in the South African savannah, S. Afr. J. Sci., 110(5/6), Art #2013-0108, 12 pages, https://doi.org/10.1590/sajs.2014/20130108, 2014

Gierens, R.T., Henriksson, S., Josipovic, M., Vakkari, V., Van Zyl, P.G., Beukes, J.P., Wood, C.R., and O'connor, E.J.: Observing continental boundary-layer structure and evolution over the South African savannah using a ceilometer, Theor. and Appl. Climatol., 1–14, https://doi.org/10.1007/s00704-018-2484-7, 2019

Gong, W., Zhang, M., Han, G., Ma, X., and Zhu, Z.: An Investigation of Aerosol Scattering and Absorption Properties in Wuhan, Central China. Atmosphere-Basel, 6, 503–520, https://doi.org/10.3390/atmos6040503, 2015

Haywood, J.M. and Boucher, O.: Estimates of the direct and indirect radiative forcing due to tropospheric aerosols: A review, Rev Geophys, 38, 513–543, https://doi.org/10.1029/1999RG000078, 2000

Haywood, J. M. and Shine, K. P.: The effect of anthropogenic sulfate and soot aerosol on the clear sky planetary radiation budget, Geophys. Res. Lett., 22, 603–606, https://doi.org/10.1029/95GL00075, 1995

Hersey, S.P., Garland, R.M., Crosbie, E., Shingler, T., Sorooshian, A., Piketh, S., and Burger, R.: An overview of regional and local characteristics of aerosols in South Africa using satellite, ground, and modelling data, Atmos. Chem. Phys., 15, 4259-4278, https://doi.org/10.5194/acp-15-4259-2015, 2015

Hirsikko, A., Vakkari, V., Tiitta, P., Manninen, H., Gagné, S., Laakso, H., Kulmala, M., Mirme, A., Mirme, S. and Mabaso, D.: Characterisation of sub-micron particle number concentrations and formation events in the western Bushveld Igneous Complex, South Africa, Atmos. Chem. Phys., 12, 3951–3967, https://doi.org/10.5194/acp-12-3951-2012, 2012

Hirsikko, A.,Vakkari, V., Tiitta, P., Hatakka, J., Kerminen, V. –M., Sundström, A.–M., Beukes, J.P., Manninen, H.E., Kulmala, M., and Laakso, L.: Multiple daytime nucleation events in semi-clean savannah and industrial environments in South Africa: analysis based on observations, Atmos. Chem. Phys., 13, 5523–5532, https://doi.org/10.5194/acp-13-5523-2013, 2013

Jaars, K., Beukes, J.P., Van Zyl, P.G., Venter, A.D., Josipovic, M., Pienaar, J.J., Vakkari, V., Aaltonen, H., Laakso, H., and Kulmala, M.: Ambient aromatic hydrocarbon measurements at Welgegund, South Africa. Atmos. Chem. Phys., 14, 7075–7089, https://doi.org/10.5194/acp-14-7075-2014, 2014

Jaars, K., Van Zyl, P.G., Beukes, J.P., Hellén, H., Vakkari, V., Josipovic, M., Venter, A.D., Räsänen, M., Knoetze, L., Cilliers, D.P., Siebert, S.J., Kulmala, M., Rinne, J., Guenther, A., Laakso, L., and Hakola, H.: Measurements of biogenic volatile organic compounds at a grazed savannah grassland agriculture landscape in South Africa, Atmos. Chem. Phys., 16, 15665–15688, https://doi.org/10.5194/acp-16-15665-2016, 2016

Jaars, K., Vestenius, M., Van Zyl, P.G., Beukes, J.P., Hellén, H., Vakkari, V., Venter, M., Josipovic, M., and Hakola, H.: Receptor modelling and risk assessment of volatile organic compounds measured at a regional background site in South Africa. Atmos. Environ., 172, 133–148, https://doi.org/10.1016/j.atmosenv.2017.10.047, 2018

Jenner, S.L. and Abiodun, B.J.: The transport of atmospheric sulfur over Cape Town, Atmos. Environ., 79, 248–260, https://doi.org/10.1016/j.atmosenv.2013.06.010, 2013

Junker, C., Jennings, S.G., and Cachier, H.: Aerosol light absorption in the North Atlantic: trends and seasonal characteristics during the period 1989 to 2003, Atmos. Chem. Phys., 6, 1913–1926, https://doi.org/10.5194/acp-6-1913-2006, 2006

Kleefeld, C., O'dowd, C.D., O'reilly, S., Jennings, S.G., Aalto, P., Becker, E., Kunz, G., and De Leeuw, G.: Relative contribution of submicron and supermicron particles to aerosol light scattering in the marine boundary layer, J. Geophys. Res., 107, 8103, https://doi.org/10.1029/2000JD000262, 2002

Korhonen, K., Giannakaki, E., Mielonen, T., Pfüller, A., Laakso, L., Vakkari, V., Baars, H., Engelmann, R., Beukes, J.P., Van Zyl, P.G., Ramandh, A., Ntsangwane, L., Josipovic, M., Tiitta, P., Fourie, G., Ngwana, I., Chiloane, K., and Komppula, M.: Atmospheric boundary layer top height in South Africa: measurements with

lidar and radiosonde compared to three atmospheric models, Atmos. Chem. Phys, 14, 4263–4278, https://doi.org/10.5194/acp-14-4263-2014, 2014

Kumar, K. R., Sivakumar, V., Reddy, R.R., Gopal, K.R., and Adesina, A.J.: Identification and classification of different aerosol types over a subtropical rural site in mpumalanga, South Africa: seasonal variations as retrieved from the AERONET sunphotometer, Aerosol Air Qual. Res., 14, 108–123, https://doi.org/10.4209/aaqr.2013.03.0079, 2014

Laakso, L., Vakkari, V., Virkkula, A., Laakso, H., Backman, J., Kulmala, M., Beukes, J.P., Van Zyl, P.G., Tiitta, P., Josipovic, M., Pienaar, J.J., Chiloane, K., Gilardoni, S., Vignati, E., Wiedensohler, A., Tuch, T., Birmili, W., Piketh, S., Collett, K., Fourie, G.D., Komppula, M., Lihavainen, H., De Leeuw, G. and Kerminen, V.-M.: South African EUCAARI measurements: seasonal variation of trace gases and aerosol optical properties, Atmos. Chem. Phys., 12, 1847–1864, https://doi.org/10.5194/acp-12-1847-2012, 2012

Laban, T.L., Van Zyl, P.G., Beukes, J.P., Vakkari, V., Jaars, K., Borduas-Denekind, N., Josipovic, M., Thompson, A.M., Kulmala, M., and Laakso, L.: Seasonal influences on surface ozone variabiliby, Atmos. Chem. Phys., 18, 15491–15514, https://doi.org/10.5194/acp-18-15491-2018, 2018

Labonne, M., Bréon, F. -M, and Chevallier, F.L.: Injection height of biomass burning aerosols as seen from a spaceborne lidar, Geophys. Res. Lett., 34, 1–5, https://doi.org/10.1029/2007GL029311, 2007

Li, Z., Xia, X., Cribb, M., Mi, W., Holben, B., Wang, P., Chen, H., Tsay, S. -C., Eck, T.F., Zhao, F., Dutton, E. G., and Dickerson, R.E.: Aerosol optical properties and their radiative effects in northern China, J. Geophys. Res. - Atmos., 112, 1–11, https://doi.org/10.1029/2006JD007382, 2008

Lihavainen, H., Hyvärinen, A., Asmi, E., Hatakka, J., and Viisanen, J.: Long-term variability of aerosol optical properties in northern Finland, Boreal Environ. Res. 20, 526–541, 2015

Loock-Hattingh, M.M., Beukes, J.P., Van Zyl, G.P., and Tiedt, L.R.: Cr(VI) and conductivity as indicators of surface water pollution from ferrochrome production inSouth Africa: Four case studies, Metall. Mater. Trans B., 46, 2315–2325, https://doi.org/10.1007/s11663-015-0395-x, 2015

Lourens, A.S., Beukes, J.P., Van Zyl, P.G., Fourie, G.D., Burger, J.W., Pienaar, J.J., Read, C.E. and Jordaan, J.H.: Spatial and temporal assessment of gaseous pollutants in the Highveld of South Africa, S. Afr. J. Sci., 107, 1–8, https://doi.org/10.4102/sajs.v107i1/2.269, 2011

Lourens, A.S.M., Butler, T.M., Beukes, J.P., Van Zyl, P.G., Fourie, G.D. and Lawrence, M.G.: Investigating atmospheric photochemistry in the Johannesburg-Pretoria megacity using a box model, S. Afr. J. Sci., 112(1/2), Art. #2015-0169, 11 pages, https://doi.org/10.17159/sajs.2016/2015-0169, 2016

Lourens, A.S., Butler, T.M., Beukes, J.P., Van Zyl, P.G., Beirle, S., Wagner, T.K., Heue, K.-P., Pienaar, J.J., Fourie, G.D., and Lawrence, M.G.: Re-evaluating the NO_2 hotspot over the South African Highveld, S. Afr. J. Sci., 108, 83–91, https://doi.org/10.4102/sajs.v108i11/12.1146, 2012

Mafusire, G., Annegarn, H.J., Vakkari, V., Beukes, J.P., Josipovic, M., Van Zyl, P.G., and Laakso, L.: Submicrometer aersols and excess CO as tracers for biomass burning air mass transport over southern Africa, J. Geophys. Res., 121, 10262–10282, https://doi.org/10.1002/2015JD023965, 2016

Maritz, P., Beukes, J.P., Van Zyl, P.G., Liousse, C., Gardrat, E., Ramandh, A. and Mkhatshwa, G.V.: Temporal and source assessments of organic and elemental carbon at sites in the northern South Africa interior, J. Atmos. Chem, https://doi.org/10.1007/s10874-020-09398-2, 2020

Mcgill, M.J., Hlavka, D.J., Hart, W.D., Welton, E.J., and Campbell, J. R.: Airborne lidar measurements of aerosol optical properties during SAFARI-2000, J. Geophys. Res-Atmos., 108, 8493, https://doi.org/10.1029/2002JD002370, 2003

Montilla, E., Mogo, S., Cachorro, V., Lopez, J., and Frutos, A. D.: Absorption, scattering and single scattering albedo of aerosols obtained from in situ measurements in the subarctic coastal region of Norway, Atmos. Chem. Phys. Discuss., 11, 2161–2182, https://doi.org/10.5194/acpd-11-2161-2011, 2011

Mucina, L. and Rutherford, M. C. (Eds.): The vegetation of South Africa, Lesotho and Swaziland, South African National Biodiversity Institute, Pretoria, South Africa, 2006

Müller, T., Laborde, M., Kassell, G., and Wiedensohler, A.: Design and performance of a three-wavelength LED-based total scatter and backscatter integrating nephelometer, Atmos. Meas. Tech., 4(6), 1291–1303, https://doi.org/10.5194/amt-4-1291-2011, 2011a

Müller, T., Henzing, J.S., De Leeuw, G., Wiedensohler, A., Alastuey, H., Bizjak, M., Collaud Coen, M., Engström, J. E., Gruening, C., Hillamo, R., Hoffer, A., Imre, K., Ivanow, P., Jennings, G., Sun, J.Y., Klaivitis, N., Karlsson, H., Komppula, M., Laj, P., Li, S.-M., Lunder, C., Marinoni, A., Martins dos Santos, S., Moerman, M., Nowak, A., Orgren, J.A., Petzold, A., Pichon, J.M., González, S.R., Sharma, S., Sheridan, P.J., Teinilä, K., Tuch, T., Viana, M., Virkkula, A., Weingartner, E., Wilhelm, R., and Wang, Y. Q.: Characterization and intercomparison of aerosol absorption photometers: result of two intercomparison workshops, Atmos. Meas. Tech., 4, 245–268, https://doi.org/10.5194/amt-4-245-2011, 2011b

Nieminen, T., Kerminen, V.-M., Petäjä, T., Aalto, P.P., Arshinov, M., Asmi, E., Baltensperger, U., Beddows, D.C.S., Beukes, J.P., Collins, D., Ding, A., Harrison, R.M., Henzing, B., Hooda, R., Hu, M., Hõrrak, U., Kivekäs, N., Komsaare, K., Krejci, R., Kristensson, A., Laakso, L., Laaksonen, A., Leaitch, W.R., Lihavainen, H., Mihalopoulos, N., Németh, Z., Nie, W., O'dowd, C., Salmal, I., Sellegri, K., Svenningsson, B., Swietlicki, E., Tunved, P., Ulevicius, V., Vakkari, V., Vana, M., Wiedensohler, A., Wu, Z., Virtanen, A., and Kulmala, K.: Global analysis of continental boundary layer new particle formation based on long-term measurements, Atmos. Chem. Phys., 18, 14737–14756, https://doi.org/10.5194/acp-18-14737-2018, 2018

Petzold, A., Schloesser, H., Sheridan, P.J., Arnott, P., Ogren, J.A. and Virkkula, A.: Evaluation of Multiangle Absorption Photometry for Measuring Aerosol Light Absorption, Aerosol Sci. Tech., 39, 40–51, https://doi.org/10.1080/027868290901945, 2005

Petzold, A., Ogren, J.A., Fiebig, M., Laj, P., Li, S.-M., Baltensperger, U., Holzer-Popp, T., Kinne, S., Pappalardo, G., and Sugimoto, N.: Recommendations for reporting "black carbon" measurements. Atmos. Chem. Phys., 13(16), 8365–8379, https://doi.org/10.5194/acp-13-8365-2013, 2013

Pretorius, I., Piketh, S., Burger, R., and Neomogus, H.: A perspective on South Africa coal fired power station emissions, J. Energy south. Afr., 26, 27–40, 2015

Queface, A.J., Piketh, S.J., Eck, T.F., Tsay, S.-C., and Mavume, A.F.: Climatology of aerosol optical properties in Southern Africa, Atmos. Environ., 45, 2910–2921, https://doi.org/10.1016/j.atmosenv.2011.01.056, 2011

Räsänen, M., Aurela, M., Vakkari, V., Beukes, J.P., Tuovinen, J.-P., Van Zyl, P.G., Josipovic, M., Venter, A.D., Jaars, K., Siebert, S.J., Laurila, T., Rinne, J., and Laakso, L.: Carbon balance of a grazed savanna grassland ecosystem in South Africa, Biogeosciences, 14, 1039–1054, https://doi.org/10.5194/bg-14-1039-2017, 2017

Reid, J.S., Eck, T.F., Christopher, S.A., Hobbs, P.V., and holben, B.: Use of the Ångström exponent to estimate the variabilty of optical and physical properties of aging smoke paricles in Brazil, J. Geophys. Res.-Atmos., 104, 27473–27489, https://doi.org/10.1029/1999JD900833, 1999

Riddle, E.E., Voss, P.B., Stohl, A., Holcomb, D., Maczka, D., Washburn, K., and Talbot, R.W.: Trajectory model validation using newly developed altitude-controlled balloons during the International Consortium for Atmospheric Research on Transport and Transformations 2004 campaign., J. Geophys. Res. Atmos. 111(D23), https://doi.org/10.1029/2006JD007456, 2006

Roy, D.P., Boschetti, L., Justice, C.O., and Ju, J.: The collection 5 MODIS burned area product – global evolution by comparison with the MODIS active fire product, Remote Sens. Environ., 112, 3690–3707, https://doi.org/10.1016/j.rse.2008.05.013, 2008

Schuster, G.L., Dubovik, O., and Holben, B.N.: Angstrom exponent and bimodal aerosol size distributions. J. Geophys. Res. Atmos., 111, https://doi.org/10.1029/2005JD006328, 2006

Seinfield, J. H. and Pandis, S.P (Eds.).: Atmospheric Chemistry and Physics: From Air Pollution to Climate Chane, John Wiley and Sons,Inc., Hoboken, New Jersey, 2016

Shen, Y., Virkkula, A., Ding, A., Wang, J., Chi, X., Nie, W., Qi, X., Huang, X., Liu, Q., Zheng, L., Xu, Z., Petäjä, T., Aalto, P. P., Fu, C., and Kulmala, M.: Aerosol optical properties at SORPES in Nanjing, east China. Atmos. Chem. Phys., 18, 5265–5292, https://doi.org/10.5194/acp-18-5265-2018, 2018

Slemr, F., Brunke, E. -G., Whittlestone, S., Zahorowski, W., Ebing-Haus, R., Kock, H. H., and Labuschagne, C.: 222 Rn-calibratedmercury fluxes from terrestrial surface of southern Africa, Atmos. Chem. Phys., 13, 6421–6428, https://doi.org/10.5194/acp-13-6421-2013, 2013

Slemr, F., Angot, H., Dommergue, A., Magand, O., Barret, M., Weigelt, A., Ebinghaus, R., Brunke, E.-G., Pfaffhuber, K.A., Edwards, G., Howard, D., Powell, J., Keywood, M., and Wang, F.: Comparison of mercury concentrations measured at several sites in the Southern Hemisphere, Atmos. Chem. Phys., 15, 3125–3133, https://doi.org/10.5194/acp-15-3125-2015, 2015

StatsSA: 2019http://www.statssa.gov.za/?page_id=1021&id=city-of-cape-town-municipality, accessed 12 April 2019

Stohl, A.: Computation, accuracy and applications of trajectories – a review and bibliography. Atmos. Environ. 32(6), 947–966, doi:10.1016/S1352-2310(97)00457-3, 1998

Swap, R.J., Annegarn, H.J., Suttles, J.T., King, M.D., Platnick, S., Privette, J.L. and Scholes, R.J.: Africa burning: a thematic analysis of the Southern African Regional Science Initiative (SAFARI 2000), J Geophys. Res. Atmos., 108, https://doi.org/10.1029/2003JD003747, 2003

Techcentral: https://techcentral.co.za/live-charts-show-awesome-power-cape-storm/74728/, accessed 12 April 2019

Tian, M., Liu, Y., Yang, F., Zhang, L., Peng, C., Chen, Y., Shi, G., Wang, H., Luo, B., Jiang, C., Li, B., Takeda, N. and Koizumi, K.: Increasing importance of nitrate formation for heavy aerosol pollution in two megacities in Sichuan Basin, southwest China, Environ. Pollut., 250, 898–905, https://doi.org/10.1016/j.envpol.2019.04.098, 2019

Tiitta, P., Vakkari, V., Croteau, P., Beukes, J.P., Van Zyl, P.G., Josipovic, M., Venter, A., Jaars, K., Pienaar, J.J., and Ng, N.: Chemical composition, main sources and temporal variability of PM 1 aerosols in southern African grassland, Atmos. Chem. Phys., 14, 1909–1927, https://doi.org/10.5194/acp-14-1909-2014, 2014

Tyson, P., Garstang, M., and Swap, R.: Large-scale recirculation of air over southern Africa, J. Appl. meteorol., 35, 2218–2236, http://dx.doi.org/10.1175/1520-0450(1996)035<2218:LSROAO>2.0.CO;2, 1996

Tyson, P.D., Preston-Whyte, R.A.: The weather and climate of southern Africa, 2nd ed. ed. Oxford University Press, Cape Town, 2000

Uria-Tellaetxe, I., and Carslaw, D.C.: Conditional bivariate probability function for source identification, Environ. Modell. Softw., 59, 1–9, http://dx.doi.org/10.1016/j.envsoft.2014.05.002, 2014

Vakkari, V., Laakso, H., Kulmala, M., Laaksonen, A., Mabaso, D., Molefe, M., Kgabi, N., and Laakso, L.: New particle formation events in semi-clean South African savannah, Atmos. Chem. Phys., 11, 3333–3346, https://doi.org/10.5194/acp-11-3333-2011, 2011

Vakkari, V., Beukes, J.P., Laakso, H., Mabaso, D., Pienaar, J.J., Kulmala, M., and Laakso, L.: Long-term observations of aerosol size distributions in semi-clean and polluted savannah in South Africa, Atmos. Chem. Phys, 13, 1751–1770, https://doi.org/10.5194/acp- 13-1751-2013, 2013

Vakkari, V., Kerminen, V.-M., Beukes, J.P., Tiitta, P., Van Zyl, P.G., Josipovic, M., Venter, A.D., Jaars, K., Worsnop, D.R., Kulmala, M., and Laakso, L.: Rapid changes in biomass burning aerosols by atmospheric oxidation. Geophys. Res. Lett., 41, 2644–2651, https://doi.org/10.1002/2014GL059396, 2014

Vakkari, V., Tiitta, P., Jaars, K., Croteau, P., Beukes, J.P., Josipovic, M., Kerminen, V.-M., Kulmala, M., Venter, A.D., Van Zyl, P.G., Worsnop, D. and Laakso, L.: Reevaluating the contribution of sulfuric acid and the origin of organic compounds in atmospheric nanoparticle growth, Geophys. Res. Lett., 42. https://doi.org/10.1002/2015GL066459, 2015

Vakkari, V., Beukes, J.P., Dal Maso, M., Aurela, M., Josipovic, M., Van Zyl, P.G.: Major secondary aerosol formation in southern Africa open biomass burning plumes, Nat. Geosci., 11, 580–583, https://doi.org/10.1038/s41561-018-0170-0, 2018

Venter, A.D., Vakkari, V., Beukes, J.P., Van Zyl, P.G., Laakso, H., Mabaso, D., Tiitta, P., Josipovic, M., Kulmala, M. and Pienaar, J.J.: An air quality assessment in the industrialised western Bushveld Igneous Complex, South Africa, S. Afr. J. Sci., 108, 1–10, https://doi.org/10.4102/sajs.v108i9/10.1059, 2012

Venter, A. D., Beukes, J.P., Van Zyl, P.G., Brunke, E.-G., Labuschagne, C., Slemr, F., Ebinghaus, R., and Kock, H.: Statistical exploration of gaseous elemental mercury (GEM) measured at Cape Point from 2007 to 2011, Atmos. Chem. Phys., 15, 10271–10280, https://doi.org/10.5194/acp-15-10271-2015, 2015

Venter, A.D., Van Zyl, P.G., Beukes, J.P., Josipovic, M., Hendriks, J., Vakkari, V., and Laakso, L.: Atmospheric trace metals measured at a regional background site (Welgegund) in South Africa, Atmos. Chem. Phys., 17, 4251–4263, https://doi.org/10.5194/acp-17-4251-2017, 2017

Venter, A.D., Van Zyl, G.P. ,Beukes, J.P., Swartz, J.-S., Josipovic, M., Vakkari, V., Laakso, L., and Kulmala, M.: Size-resolved characteristics of inorganic ionic species in atmopheric aerosols at a regional background site on the South African Highveld, J. Atmos. Chem., 1–20, https://doi.org./10.1007/s10874-018-9378-z, 2018

Virkkula, A., Backman, J., Aalto, P.P., Hulkkonen, M., Riuttanen, L., Nieminem, T., Dal Maso, M., Sogacheva, L., De Leeuw, G., and Kulmala, M.: Seasonal cycle, size, dependencies, and source analysis of aerosol optical properties at the SMEAR II measurement station in Hyytiala, Finland, Atmos. Chem. Phys., 11, 4445–4468, https://doi.org/10.5194/acp-11-4445-2011, 2011

Xu, J., Bergin, M. H., Yu, X., Liu, G., Zhao, J., Carrico, C. M., and Baumann, K.: Measurement of aerosol chemical, physical and radiative properties in the Yangtze delta region of China, Atmos. Eviron., 36, 161–173, https://doi.org/10.1016/S1352-2310(01)00455-1, 2002

Xu, J., Bergin, M. H., Greenwald, R., Schauer, J.J., Shafer, M.M., Jaffrezo, J.L., and Aymoz, G.: Aerosol chemical, physical, and radiative characteristics near a desert source region of northwest China during ACE-Asia, J. Geophys. Ress-Atmos., 109, 1–14, https://doi.org/10.1029/2003JD004239, 2004

Yan, P., Tang, J., Huang, J., Mao, J.T., Zhou, X.J., Liu, Q., Wang, Z.F., Zhou, H.G.: The measurement of aerosol optical properties at a rural site in Northern China, Atmos. Chem. Phys., 8, 2229–2242, https://doi.org/10.5194/acp-8-2229-2008, 2008